PHYSICAL REVIEW D **94,** 095016 (2016)

Neutrino jets from high-mass W_R gauge bosons in TeV-scale left-right symmetric models

Manimala Mitra,[1,2,*] Richard Ruiz,[2,†] Darren J. Scott,[2,‡] and Michael Spannowsky[2,§]

[1]*Department of Physics, Indian Institute of Science Education and Research Mohali (IISER Mohali), Sector 81, SAS Nagar, Manauli 140306, India*

[2]*Institute for Particle Physics Phenomenology (IPPP), Department of Physics, Durham University, Durham DH1 3LE, United Kingdom*

(Received 29 July 2016; published 15 November 2016)

We reexamine the discovery potential at hadron colliders of high-mass right-handed (RH) gauge bosons W_R—an inherent ingredient of left-right symmetric models (LRSM). We focus on the regime where the W_R is very heavy compared to the heavy Majorana neutrino N, and we investigate an alternative signature for $W_R \to N$ decays. The produced neutrinos are highly boosted in this mass regime. Subsequently, their decays via off-shell W_R bosons to jets, i.e., $N \to \ell^\pm jj$, are highly collimated, forming a single neutrino jet (j_N). The final-state collider signature is then $\ell^\pm j_N$, instead of the widely studied $\ell^\pm \ell^\pm jj$. Present search strategies are not sensitive to this hierarchical mass regime due to the breakdown of the collider signature definition. We take into account QCD corrections beyond next-to-leading order (NLO) that are important for high-mass Drell-Yan processes at the 13 TeV Large Hadron Collider (LHC). For the first time, we evaluate W_R production at NLO with threshold resummation at next-to-next-to-leading logarithm (NNLL) matched to the threshold-improved parton distributions. With these improvements, we find that a W_R of mass $M_{W_R} = 3(4)[5]$ TeV and mass ratio of $(m_N/M_{W_R}) < 0.1$ can be discovered with a 5–6σ statistical significance at 13 TeV after $10(100)[2000]$ fb^{-1} of data. Extending the analysis to the hypothetical 100 TeV Very Large Hadron Collider (VLHC), 5σ can be obtained for W_R masses up to $M_{W_R} = 15(30)$ with approximately 100 fb^{-1} (10 ab^{-1}). Conversely, with $0.9(10)[150]$ fb^{-1} of 13 TeV data, $M_{W_R} < 3(4)[5]$ TeV and $(m_N/M_{W_R}) < 0.1$ can be excluded at 95% C.L.; with 100 fb^{-1} (2.5 ab^{-1}) of 100 TeV data, $M_{W_R} < 22(33)$ TeV can be excluded.

DOI: 10.1103/PhysRevD.94.095016

I. INTRODUCTION

The observation of nonzero neutrino masses m_ν, which have hierarchically smaller masses than all other elementary fermions in the Standard Model of Particle Physics (SM), and their nontrivial mixing provide unambiguous experimental evidence of physics beyond the SM (BSM). The natural explanation for such tiny masses is the so-called seesaw mechanism, where eV neutrino masses are generated from the $(B-L)$-violating operators at dimension 5 [1,2]. At tree level, these operators can be generated by minimally extending [3] the SM field contents by right-handed (RH) neutrinos N_R (type I) [4–9], scalar $\mathrm{SU}(2)_L$ triplets Δ_L (type II) [10–13], or fermionic $\mathrm{SU}(2)_L$ triplets Σ (type III) [14]. If kinematically accessible, these states can be observed at the 13 TeV Large Hadron Collider (LHC) or a hypothetical 100 TeV Very Large Hadron Collider (VLHC) [15,16], thus giving conclusive evidence of the mass generation mechanism. For reviews of TeV-scale seesaw models and their phenomenology, see Ref. [17].

An appealing renormalizable framework in which both types I and II seesaw models can be embedded is the left-right symmetry model (LRSM) [18–21]. This is based on the gauge group

$$\mathrm{SU}(3)_c \otimes \mathrm{SU}(2)_L \otimes \mathrm{SU}(2)_R \otimes \mathrm{U}(1)_{B-L} \qquad (1)$$

and postulates the restoration of parity symmetry at high energies. In addition to the SM particle content, the model consists of three generations of N_R, one Δ_L, and an $\mathrm{SU}(2)_R$ triplet scalar Δ_R, all with nontrivial charges under the $B-L$ symmetry. After Δ_R acquires a vacuum expectation value (VEV) v_R, much larger than the electroweak (EW) scale, $v_{\mathrm{SM}} \approx 246$ GeV, the $SU(2)_R \times U(1)_{B-L}$ symmetry breaks down to the $U(1)_Y$ of the SM. Subsequently, the neutrinos N_R and gauge bosons W_R and Z_R acquire masses M_R, M_{W_R} and M_{Z_R}, respectively, that are proportional to v_R. While the masses of the gauge bosons depend on the weak gauge coupling $g_R = g$, the masses of N_R are dependent on the Yukawa coupling f_R of the Δ_R and lepton doublet interaction. The RH neutrino also interacts with the SM neutrino via its Yukawa interaction, generating Dirac masses M_D after EW symmetry breaking (EWSB). For the Majorana mass M_R much heavier than the Dirac mass

*manimala.mitra@durham.ac.uk
†richard.ruiz@durham.ac.uk
‡d.j.scott@durham.ac.uk
§michael.spannowsky@durham.ac.uk

M_D, a type I seesaw mechanism is triggered [4–9], giving rise to Majorana masses for light neutrinos ν_m with $m_\nu \sim M_D^2/M_R$ and heavy neutrinos N with $m_N \sim M_R$. As no symmetry relates the RH gauge and triplet Yukawa couplings, the W_R and heavy neutrino may have widely separated masses, and this offers a wide parameter space to test the LRSM.

The LRSM model can be tested either indirectly, through low energy experiments [22–36], or directly, through searches at high energy colliders [16,30,37–53] (and references therein). In this work, we focus on the direct detection of the W_R and N. For $M_{W_R} > m_N$, the hallmark hadron collider test of the LRSM is the spectacular lepton number (L) violating process [37]

$$q_1\bar{q}_2 \to W_R^\pm \to N_R\ell_1^\pm \to \ell_1^\pm\ell_2^\pm W_R^{\mp *} \to \ell_1^\pm\ell_2^\pm q_1'\bar{q}_2'. \quad (2)$$

The process, shown in Fig. 1, has been studied extensively. Searches by the ATLAS [54] and CMS [55] collaborations have excluded regions of the (M_{W_R}, m_N) parameter space for M_{W_R} (m_N) up to several TeV (hundred GeV) [56,57]. However, for hierarchical masses, i.e., $(m_N/M_{W_R}) < 0.1$, the present search strategy is no longer sensitive. Complementary dijet searches have similarly excluded M_{W_R} below 2.5 – 3.5TeV [58–60].

In light of such stringent bounds, we reexamine the discovery potential of high-mass W_R at hadron colliders. We focus on the situation where N are hierarchically lighter than W_R, i.e., $(m_N/M_{W_R}) < 0.1$. In the process $pp \to W_R \to N\ell$, this leads to boosted N with transverse momentum $p_T^N \sim M_{W_R}/2$. The decay products of N, which proceed dominantly through far off-shell W_R to quarks, i.e., $N \to W_R^*\ell \to q\bar{q}'\ell$, are subsequently collimated with parton separations scaling as $\Delta R_{ij} \sim 2m_N/p_T^N \sim 4m_N/M_{W_R}$. Hence, for $m_N/M_{W_R} \lesssim 0.1$, one has $\Delta R_{ij} \lesssim 0.4$, which falls below the electron isolation threshold in standard high-p_T lepton searches at the 13 TeV LHC [62]. Indeed, the LHC sensitivity of Eq. (2) for such (M_{W_R}, m_N) is considerably weaker, particularly in the electron channel [54]. This deficiency has been noted before, e.g., Refs. [38,41,51,63], but never explored in substantial detail.

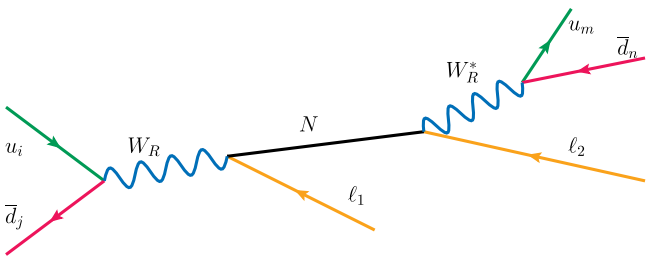

FIG. 1. Born diagram of W_R production in hadron collisions and decay via N to leptons and quarks. Figures are drawn using JaxoDraw [61].

After hadronization, the decay products of N do not appear as individual, isolated objects, but instead as a single neutrino jet j_N. This is akin to the formation of top jets from boosted top quarks [64–68]. Thus, for $m_N \ll M_{W_R}$, $W_R - N$ production and decay appear in pp collisions as the distinctive

$$pp \to W_R^\pm \to \ell^\pm j_N. \quad (3)$$

Despite the inclusive channel's simplified topology, and hence larger SM backgrounds, it inherits much of the strong discriminating power of Eq. (2), including a fully reconstructible final state and no missing p_T (MET), other than the hadronization and detector effects. We consider a search strategy for $W_R - N$ production and decay when $M_{W_R} > 3$ TeV and $(m_N/M_{W_R}) < 0.1$, while using a simple set of kinematical cuts on the effective two-body final state. We explore the discovery potential of observing Eq. (3) for the c.m. energies $\sqrt{s} = 13$ and 100 TeV, relevant for the LHC and VLHC.

Furthermore, determining if the W_R gauge coupling g_R equals the SM weak coupling g, a postulate of Eq. (1), requires precision knowledge of W_R production rates. However, for such large W_R masses, QCD corrections beyond next-to-leading order (NLO) are important at 13 TeV because of soft gluon radiation off initial-state partons. In light of this, we also calculate, for the first time, W_R production at NLO with threshold resummation at next-to-next-to-leading logarithm (NNLL) matched to threshold-improved parton distributions functions (PDFs) [69,70]. Previous predictions [60,71,72] have considered threshold resummation up to next-to-leading logarithm (NLL) [60] but never matched to resummed PDFs. NLO + NNLL contributions improve the Born (NLO)-level predictions for $M_{W_R} = 4$–5 TeV by 40–140(4–72)% at 13 TeV LHC.

With these improvements, we find that a W_R of mass $M_{W_R} = 3(4)[5]$ TeV and $(m_N/M_{W_R}) < 0.1$ can be discovered with a 5–6σ statistical significance at 13 TeV after 10(100)[2000] fb^{-1}. At 100 TeV with 0.1(10) ab^{-1}, the 5σ reach extends to $M_{W_R} = 15(30)$ TeV. Conversely, with 0.9(10)[150] fb^{-1} of 13 TeV data, $M_{W_R} < 3(4)[5]$ TeV and $(m_N/M_{W_R}) < 0.1$ can be excluded at 95% confidence level (C.L.); with 100 fb^{-1} (2.5 ab^{-1}) of 100 TeV data, $M_{W_R} < 22(33)$ TeV can be excluded.

Our paper is organized as follows: In Sec. II, we briefly review the minimal LRSM (MLRSM) and current constraints. In Sec. III, we present predictions up to NLO + NNLL for $W_R - N$ production and decay rates at hadron colliders. We explore the phenomenology of boosted heavy neutrinos and present our signal-vs-background analysis in Sec. IV. In Sec. V, we summarize and conclude. We relegate technical details of our resummation

calculation to Appendix A and implementation of the LRSM model files by Ref. [73] to Appendix B.

II. MINIMAL LEFT-RIGHT SYMMETRIC MODEL

Here, we briefly review the main aspects of the MLRSM relevant to our study. For an expanded discussion, see, e.g., Ref. [24]. In Secs. II A and II B, we address the masses of W_R and N. In Sec. II C, experimental constraints are reviewed. We reserve discussing the model's scalar potential and its implementation into publicly available simulation model files [73] for Appendix B. As we use the files of Ref. [73], we adopt their notation.

The MLRSM [18–20] is based on the extended gauge group

$$\mathrm{SU}(3)_c \otimes \mathrm{SU}(2)_L \otimes \mathrm{SU}(2)_R \otimes \mathrm{U}(1)_{B-L}. \tag{4}$$

In addition to the SM fermion field content, there are three generations of RH neutrinos N_R. Quark and lepton multiplets are assigned the following gauge group representations:

$$\begin{aligned} Q_{L,i} &= \begin{pmatrix} u_L \\ d_L \end{pmatrix}_i : \left(\mathbf{3},\mathbf{2},\mathbf{1},\frac{1}{3}\right), \\ Q_{R,i} &= \begin{pmatrix} u_R \\ d_R \end{pmatrix}_i : \left(\mathbf{3},\mathbf{1},\mathbf{2},\frac{1}{3}\right), \\ \psi_{L,i} &= \begin{pmatrix} \nu_L \\ e_L \end{pmatrix}_i : (\mathbf{1},\mathbf{2},\mathbf{1},-1), \\ \psi_{R,i} &= \begin{pmatrix} N_R \\ e_R \end{pmatrix}_i : (\mathbf{1},\mathbf{1},\mathbf{2},-1). \end{aligned} \tag{5}$$

In the above, $i = 1, \ldots, 3$ is the family index. Note that $(B-L)$ charges are normalized such that the electric charge is given by $Q = I_{3L} + I_{3R} + (B-L)/2$, with $I_{3L(3R)}$ being the third isospin components of $\mathrm{SU}(2)_{L(R)}$. The scalar sector consists of the following multiplets:

$$\begin{aligned} \Phi &= \begin{pmatrix} \phi_1^0 & \phi_2^+ \\ \phi_1^- & \phi_2^0 \end{pmatrix} : (\mathbf{1},\mathbf{2},\mathbf{2},0), \\ \Delta_L &= \begin{pmatrix} \Delta_L^+/\sqrt{2} & \Delta_L^{++} \\ \Delta_L^0 & -\Delta_L^+/\sqrt{2} \end{pmatrix} : (\mathbf{1},\mathbf{3},\mathbf{1},2), \\ \Delta_R &= \begin{pmatrix} \Delta_R^+/\sqrt{2} & \Delta_R^{++} \\ \Delta_R^0 & -\Delta_R^+/\sqrt{2} \end{pmatrix} : (\mathbf{1},\mathbf{1},\mathbf{3},2). \end{aligned} \tag{6}$$

At a scale much higher than the EW scale, Δ_R acquires a VEV $v_R = \sqrt{2}\langle\Delta_R\rangle$. This triggers spontaneous breaking of the LR and $(B-L)$ symmetries, and reduces Eq. (4) to the SM gauge group, i.e., $\mathrm{SU}(2)_R \times \mathrm{U}(1)_{B-L} \to \mathrm{U}(1)_Y$. The bidoublet Φ is responsible for Dirac masses and EWSB after it acquires the VEVs $\langle\Phi\rangle = \mathrm{diag}(k_1, k_2)/\sqrt{2}$, where

$$k_\pm^2 \equiv k_1^2 \pm k_2^2 \quad \text{and} \quad k_+ = v_{\mathrm{SM}} \approx 246\ \mathrm{GeV}. \tag{7}$$

In the absence of fine-tuning, k_1, k_2 naturally scale as

$$\frac{k_2}{k_1} \sim \frac{m_b}{m_t} \ll 1. \tag{8}$$

Note that Δ_L can also acquire a VEV $v_L = \sqrt{2}\langle\Delta_L\rangle$. However, precision measurements of the ρ/T parameter indicate that v_L is much smaller than the EW scale [22,25]. For simplicity, we take v_R and $k_{1,2}$ to be real, i.e., no CP violation, and $v_L = 0$.

A. Charged gauge boson masses

After LR and EWSB, the charged vector boson (squared) mass matrix in the gauge, i.e., (W_L, W_R), basis is given by

$$\mathcal{M}_W = \frac{g^2}{4}\begin{pmatrix} k_1^2 + k_2^2 + 2v_L^2 & 2k_1k_2 \\ 2k_1k_2 & k_1^2 + k_2^2 + 2v_R^2 \end{pmatrix}. \tag{9}$$

The gauge states are related to the mass eigenstates, i.e., (W_1, W_2) with $M_{W_2} > M_{W_1}$, by

$$\begin{pmatrix} W_1 \\ W_2 \end{pmatrix} = \begin{pmatrix} \cos\xi & \sin\xi \\ -\sin\xi & \cos\xi \end{pmatrix}\begin{pmatrix} W_L \\ W_R \end{pmatrix}, \tag{10}$$

where the $W_L - W_R$ mixing parameter ξ is

$$\tan 2\xi = \frac{2k_1k_2}{v_R^2 - v_L^2}. \tag{11}$$

Under the VEV hierarchy

$$v_R \gg k_+ \gtrsim k_1 \gtrsim k_- \gg k_2 \gg v_L \sim 0, \tag{12}$$

the vector boson masses simplify to

$$M_{W_1} \approx M_{W_L} = \frac{g}{2}k_+ \quad \text{and} \quad M_{W_2} \approx M_{W_R} = \frac{g}{\sqrt{2}}v_R, \tag{13}$$

implying that the $W_1(W_2)$ mass state is closely aligned with the $W_L(W_R)$ gauge state. Hence, for the remainder of the text, we refer to $W_1(W_2)$ as $W_L(W_R)$.

B. Neutrino masses

The leptonic Yukawa couplings for generations i and j are given by

$$\begin{aligned} \mathcal{L}_Y = &-h_{ij}\bar{\psi}_{L_i}\Phi\psi_{R_j} - \tilde{h}_{ij}\bar{\psi}_{L_i}\tilde{\Phi}\psi_{R_j} - f_{L_{ij}}\psi_{L_i}^{\mathsf{T}}Ci\sigma_2\Delta_L\psi_{L_j} \\ &- f_{R_{ij}}\psi_{R_i}^{\mathsf{T}}Ci\sigma_2\Delta_R\psi_{R_j} + \mathrm{H.c.}, \end{aligned} \tag{14}$$

where C denotes the charge conjugation operator and $\tilde{\Phi} = \sigma_2\Phi^*\sigma_2$. After LR and EWSB, RH Majorana, LH Majorana, and Dirac neutrino mass matrices, respectively, of the form

$$M_R = \sqrt{2} v_R f_R,$$
$$M_L = \sqrt{2} v_L f_L,$$
$$M_D = \frac{1}{\sqrt{2}}(k_1 h + k_2 \tilde{h}), \tag{15}$$

are spontaneously generated. The 3×3 matrices in Eq. (15) can be combined such that in the gauge basis, i.e., $(\nu_{L1}, \ldots, N^c_{R1}, \ldots)$, the 6×6 neutrino mass matrix is given by

$$\mathcal{M}_\nu = \begin{pmatrix} M_L & M_D \\ M_D^{\mathsf{T}} & M_R \end{pmatrix} \tag{16}$$

and can be diagonalized via the unitary matrix $\tilde{V}$:

$$\mathcal{M}_\nu^{\text{diag}} = \tilde{V}^{\mathsf{T}} \mathcal{M}_\nu \tilde{V} = \begin{pmatrix} M_\nu^{\text{diag}} & \mathbf{0} \\ \mathbf{0} & M_N^{\text{diag}} \end{pmatrix}. \tag{17}$$

$M_\nu^{\text{diag}} = \text{diag}(m_1, m_2, m_3)$ and $M_N^{\text{diag}} = \text{diag}(m_{N_1}, m_{N_2}, m_{N_3})$ are the light neutrino and heavy neutrino masses, respectively. For the VEV hierarchy of Eq. (12), $\tilde{V}$ is [74,75]

$$\tilde{V} = \begin{pmatrix} (\mathbf{1} + \zeta^* \zeta^{\mathsf{T}})^{-1/2} & \zeta^* (\mathbf{1} + \zeta^{\mathsf{T}} \zeta^*)^{-1/2} \\ -\zeta^{\mathsf{T}} (\mathbf{1} + \zeta^* \zeta^{\mathsf{T}})^{-1/2} & (\mathbf{1} + \zeta^{\mathsf{T}} \zeta^*)^{-1/2} \end{pmatrix} \begin{pmatrix} U_L & \mathbf{0} \\ \mathbf{0} & Y_R \end{pmatrix} \equiv \begin{pmatrix} U & V \\ X & Y \end{pmatrix}, \tag{18}$$

where $\zeta^* = M_D M_R^{-1}$ and U_L, Y_R are unitary matrices that diagonalize $\tilde{M}_\nu$ and $\tilde{M}_R$:

$$M_\nu^{\text{diag}} = U_L^{\mathsf{T}} \tilde{M}_\nu U_L \quad \text{and} \quad M_N^{\text{diag}} = Y_R^{\mathsf{T}} \tilde{M}_N Y_R. \tag{19}$$

$\tilde{M}_\nu$ and $\tilde{M}_N$ are related to the mass matrices in Eq. (15) by the seesaw relations [4–13]

$$\tilde{M}_\nu \simeq M_L - M_D M_R^{-1} M_D^{\mathsf{T}} \quad \text{and} \quad \tilde{M}_N \simeq M_R. \tag{20}$$

In the notation of Refs. [41,76], after rotating the charged leptons from the flavor basis into the mass basis, which for simplicity we take to be a trivial rotation, the $U_{\ell \nu_m}(Y_{\ell N_{m'}})$ of Eq. (18) denotes the large $\mathcal{O}(1)$ mixing between the LH (RH) lepton flavor state $\ell (\ell = e, \mu, \tau)$ and light (heavy) neutrino mass eigenstate $\nu_m (N_{m'})$. Similarly, $V_{\ell N_{m'}}(X_{\ell \nu_m})$ denotes the suppressed $\mathcal{O}(m_\nu/m_N)$ mixing between the LH (RH) lepton flavor state ℓ and heavy (light) neutrino mass eigenstate $N_{m'}(\nu_m)$.

C. Experimental constraints

Here, we review the most stringent constraints on the MLRSM.

(1) *Collider bounds on (M_{W_R}, m_N) from $\ell^\pm \ell^\pm jj$ searches*: Searches by the ATLAS experiment for $pp \to e^\pm e^\pm jj (\mu^\pm \mu^\pm jj)$ mediated by W_R and N exclude the following at $\sqrt{s} = 8$ TeV [54]:

$$M_{W_R} \lesssim 1.5(2.7) \text{ TeV} \quad \text{at } 95\% \text{ C.L.} \quad \text{with} \quad \mathcal{L} = 20.3 \text{ fb}^{-1}. \tag{21}$$

The sensitivity disparity is due to a failing isolated electron-jet criterion when $m_N/M_{W_R} \lesssim 0.1$ [54] and is the point of our study. Limits from CMS are comparable [55].

(2) *Collider bounds on M_{W_R} from dijet searches*: Searches by the ATLAS (CMS) experiment for a sequential SM $W' \to jj$ exclude the following at $\sqrt{s} = 13$ TeV [58,59]:

$$M_{W'_{\text{SSM}}} \lesssim 2.6(2.6) \text{ TeV} \quad \text{at } 95\% \text{ C.L.} \quad \text{with} \quad \mathcal{L} = 3.6(2.4) \text{ fb}^{-1}. \tag{22}$$

(3) *Limits on W_R and Higgs masses from neutral hadron transitions*: Analyses of $\Delta F = 2$ transitions in neutral K and $B_{d,s}$ systems and neutron EDM assuming generalized charge (parity) in the MLRSM exclude the following [34,35]:

$$M_{W_R} > 2.9\text{–}20 \text{ TeV} \quad \text{at } 95\% \text{ C.L.}, \tag{23}$$

$$m_{\text{FCNH}} > 20 \text{ TeV} \quad \text{at } 95\% \text{ C.L.}, \tag{24}$$

where the range over M_{W_R} is based on theoretical arguments and m_{FCNH} is the mass of the lightest Higgs mediating flavor changing neutral transitions.

(4) *Searches for $0\nu\beta\beta$*: In MLRSM, the gauge boson W_R together with N_i can give a saturating contribution in $0\nu\beta\beta$. Nonobservation of this LNV process hence constrains the masses of W_R and N_i as $\sum_i \frac{Y_{ei}^2}{M_i M_{W_R}^4} \leq (0.082\text{–}0.076) \text{ TeV}^{-5}$, using the 90% C.L. half-life limit from KamLAND-Zen $T_{1/2}^{0\nu} \geq 1.07 \times 10^{26}$ yrs [77]. For an M_{W_R} of 3 TeV (5 TeV), this implies a lower limit on the $m_N \geq 150\text{–}162$ GeV (19.5–21 GeV) [31].

III. PROPERTIES OF W_R AND N AT HADRON COLLIDERS

In this section, we present production and decay rates of W_R and N to leptons and jets, with $m_N \ll M_{W_R}$, at the 13 TeV LHC and 100 TeV VLHC.

In the MLRSM, the W_R interaction with quarks is given by the Lagrangian

$$\mathcal{L}_{W_R-q-q'} = \frac{-g}{\sqrt{2}} \sum_{i,j=u,d,\ldots} \bar{u}_i V_{ij}^{\mathrm{CKM}'} W_{R\mu}^{+} \gamma^{\mu} P_R d_j + \mathrm{H.c.}, \quad (25)$$

where $u_i(d_j)$ is an up- (down-) type quark of flavor $i(j)$, $V_{ij}^{\mathrm{CKM}'}$ is the RH Cabbibo-Kobayashi-Masakawa (CKM) matrix, and $P_{R(L)} = \frac{1}{2}(1 \pm \gamma^5)$ denotes the RH (LH) chiral projection operator. We assume four massless quarks and take $V_{ij}^{\mathrm{CKM}'}$ to be diagonal with unit entries.

The W_R coupling to six heavy $(N_{m'})$ and light (ν_m) neutrinos is parametrized by [41,76]

$$\mathcal{L}_{W_R-\ell-\nu/N} = \frac{-g}{\sqrt{2}} \sum_{\ell=e,\mu,\tau} \left[\sum_{m=1}^{3} \bar{\nu_m^c} X_{\ell m} + \sum_{m'=4}^{6} \overline{N_{m'}} Y_{\ell m'} \right] \times W_{R\mu}^{+} \gamma^{\mu} P_R \ell^{-} + \mathrm{H.c.}, \quad (26)$$

where mixing matrices $X_{\ell m}$ and $Y_{\ell m'}$ are defined in Sec. II B. We consider only the lightest heavy neutrino, denoted simply by N, and neglect heavier mass eigenstates. For simplicity, we assume diagonal neutrino mixing with maximal coupling to electron-flavor leptons:

$$|Y_{eN}| = 1, \qquad |Y_{\mu N}| = |Y_{\tau N}| = |X_{\ell m}| = 0. \quad (27)$$

Choosing instead maximal coupling to muons, i.e., $|Y_{\mu N}| = 1$, or large $e-\mu$ mixing, i.e., $|Y_{eN}| \sim |Y_{\mu N}|$, has little impact on our analysis due to the long lifetime of the muon. On the other hand, the $\tau\ell$ final state requires specialized cuts to account for τ decays to light neutrinos. For more details, see Sec. IV A.

For numerical results, SM inputs are taken from the 2014 Particle Data Group [78]:

$$\alpha^{\overline{\mathrm{MS}}}(M_Z) = 1/127.940, \quad M_Z = 91.1876\ \mathrm{GeV}, \quad \sin^2_{\overline{\mathrm{MS}}}(\theta_W; M_Z) = 0.23126. \quad (28)$$

PDFs and $\alpha_s(\mu_r)$ are extracted using the LHAPDF 6.1.6 libraries [79]. The factorization (μ_f) and renormalization (μ_r) scales are set to $\mu_0 = M_{W_R}$ everywhere. For LO- and NLO-accurate calculations, we use the NNPDF 3.0 NLO $n_f = 4$ (`lhaid=260400`) PDF set [80]. For NLO + NNLL calculations, we use the threshold-improved NNPDF 3.0 NNLO + NNLL PDF set [69]. This choice follows from the unavailability of a NLO + NNLL PDF set and our desire to ascertain the effects of resummation at NNLL. Formally, the induced uncertainties from our PDF mismatching in the LO and NLO + NNLL calculations are $\mathcal{O}(\alpha_s)$ and $\mathcal{O}(\alpha_s^2)$, respectively, and beyond our claimed accuracy. Numerically, this leads to LO cross sections that are 10% smaller than those calculated with LO PDFs.

For additional computational details, see Appendix A.

A. W_R production at NLO + NNLL

At fixed order (FO) accuracy, we calculate the inclusive production cross section for

$$pp \to W_R^{\pm} + X, \quad (29)$$

where X is anything, via the usual application of the collinear factorization theorem:

$$\sigma^{\mathrm{FO}}(pp \to W_R + X) = \sum_{a,b=q,\bar{q}',g} \int_{\tau_0}^{1} d\tau \mathcal{L}_{ab}(\tau,\mu_f) \hat{\sigma}^{\mathrm{FO}}(ab \to W_R), \quad \tau_0 \equiv \frac{M_{W_R}^2}{s}. \quad (30)$$

The luminosity $\mathcal{L}(\tau)$ of parton pair ab in pp collisions given by

$$\mathcal{L}_{ab}(\tau,\mu_f) = \frac{1}{1+\delta_{ab}} \int_{\tau}^{1} \frac{d\xi_1}{\xi_1} [f_{a/p}(\xi_1,\mu_f) f_{b/p}(\xi_2,\mu_f) + f_{a/p}(\xi_2,\mu_f) f_{b/p}(\xi_1,\mu_f)], \quad (31)$$

$$\xi_2 \equiv \frac{\tau}{\xi_1}. \quad (32)$$

The PDFs $f_{a/p}(\xi_i,\mu_f)$ represent the likelihood of observing parton a in proton p possessing a longitudinal momentum fraction $\xi_i = E_a/E_{p_i} = p_a^z/E_{p_i}$, and (re)sum arbitrary collinear parton emissions up to a factorization scale μ_f. The partonic c.m. energy $\sqrt{\hat{s}}$ is related to the hadronic (beam) c.m. energy $\sqrt{s}$ by the hadronic threshold variable

$$\tau = \xi_1 \xi_2 = \frac{\hat{s}}{s}, \qquad \tau_0 \le \tau < 1, \quad (33)$$

and it extends to the kinematic threshold τ_0, below which Eq. (29) is kinematically forbidden.

Partonic scattering rates $\hat{\sigma}$ are evaluated via helicity amplitudes and use the CUBA libraries [81] to handle Monte Carlo integration. NLO in QCD corrections are obtained using the phase space slicing method [82–85], and they exploit factorization properties of Drell-Yan (DY) currents; see appendixes of Refs. [85,86]. LO and NLO results are checked against the literature [60,71,73] and MG5_aMC@NLO v2.3.3 (MG5) [87] assuming $M_{W_R} = M_W$.

Beyond FO, Eq. (30) can be generalized [88–90] to include the arbitrary, initial-state emission of soft gluons, i.e., with energies much smaller than the hard scattering process scale Q. The interpretation of $\hat{\sigma}$ also generalizes to include both the hard process,

$$q\bar{q}' \to W_R^{\pm} \quad \text{with} \quad Q = M_{W_R}, \quad (34)$$

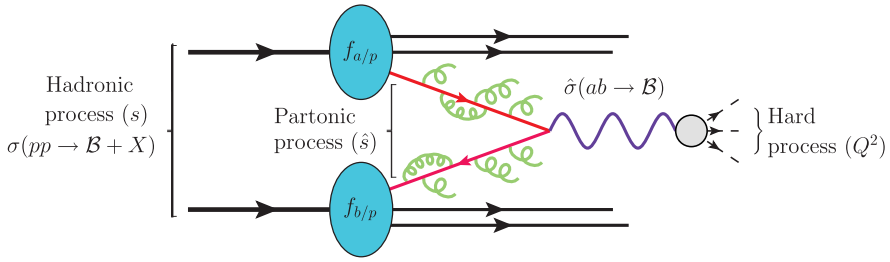

FIG. 2. Schematic definitions of the hadronic (s), partonic ($\hat{s}$) and hard scatting (Q^2) components for inclusive production of a generic color-singlet boson $\mathcal{B}$ in pp collisions.

and the factorized soft radiation off the $q, \bar{q}'$ initial states. Schematically, the definitions of the hadronic, partonic, and hard components for the inclusive production of a generic color-singlet boson $\mathcal{B}$ are drawn in Fig. 2. Necessarily, the inequality $s > \hat{s} \geq Q^2$ holds.

Soft radiation becomes important when the hard scale approaches the partonic scale, i.e., when the partonic threshold variable z approaches 1:

$$z \equiv \frac{Q^2}{\hat{s}} = \frac{M_{W_R}^2}{\hat{s}} = \frac{\tau_0}{\tau} \to 1. \tag{35}$$

In this kinematic regime, which can be satisfied at $Q^2 \ll s$ as in Higgs production via GF or when $Q^2 \sim s$ as in the present case of high-mass DY, soft radiation gives rise to numerically large logarithms that require resummation in order to restore the perturbativity of Eq. (30).

To carry out the resummation, we follow the procedure (and largely notations) of Refs. [91–93] and write a generalized form of Eq. (30) in terms of τ, z, and τ_0:

$$\sigma^{\mathrm{FO}}(pp \to W_R + X) = \sum_{a,b=q,\bar{q}',g} \int_{\tau_0}^1 d\tau \int_0^1 dz \delta\left(z - \frac{\tau_0}{\tau}\right) \mathcal{L}_{ab}(\tau) \hat{\sigma}_{ab}^{\mathrm{FO}}(ab \to W_R). \tag{36}$$

For inclusive W_R production, $\hat{\sigma}^{\mathrm{FO}}$ can be expressed as

$$\hat{\sigma}_{ab}^{\mathrm{FO}} \equiv \hat{\sigma}^{\mathrm{FO}}(ab \to W_R) = \sigma_0 \times z \times \Delta_{ab}^{\mathrm{FO}}(z). \tag{37}$$

The constant term σ_0 for gauge coupling $g_R^2 = g^2 = 4\pi\alpha/\sin^2\theta_W$ is

$$\sigma_0 = \frac{g_R^2 \pi |V_{ab}^{\mathrm{CKM}'}|^2}{4 N_c M_{W_R}^2}, \tag{38}$$

and it is related to the usual LO partonic formula by

$$\hat{\sigma}^{\mathrm{LO}}(ab \to W_R) = \sigma_0 \times M_{W_R}^2 \times \delta(\hat{s} - M_{W_R}^2) = \sigma_0 \times z \times \delta(1 - z). \tag{39}$$

Hence, one may identify up to $\mathcal{O}(\alpha_s)$, $\Delta_{q\bar{q}'}^{\mathrm{FO}}(z) \approx \delta(1-z) + \mathcal{O}(\alpha_s)$.

If working with pQCD, the threshold resummed cross section can be efficiently obtained after writing the hadronic cross section in so-called Mellin space. For the function $h(x)$, the Nth moments of its Mellin transform and inverse Mellin transform with respect to x are

$$h_N \equiv \mathcal{M}[h(x); N] = \int_0^1 dx x^{N-1} h(x), \tag{40}$$

$$h(x) = \mathcal{M}^{-1}[h_N; x] = \frac{1}{2\pi i} \int_{c-i\infty}^{c+i\infty} dN x^{-N} h_N, \tag{41}$$

where $c \in \mathbb{R}$ is to the right of all singularities in h_N. The Mellin transform of Eq. (36) at LO with respect to τ_0 gives

$$\sigma_N^{\mathrm{LO}} = \int_0^1 d\tau_0 \tau_0^{N-1} \times \sigma^{\mathrm{LO}}(\tau_0) = \sigma_0 \mathcal{L}_{q\bar{q}',(N+1)} \times \Delta_{q\bar{q}',(N+1)}^{\mathrm{LO}}, \tag{42}$$

revealing an explicit factorization into a product of the luminosity and soft coefficient, normalized by the Born weight σ_0. We drop the summation over $a, b = g$ as the $gq, g\bar{q}'$, and gg initial states do not contribute to W_R production at LO.

The advantage of working in Mellin space is this explicit factorization. Exploiting that in the soft limit gauge radiation amplitudes reduce to their color-connected Born amplitudes, resummation reduces to the simple procedure of replacing the LO soft coefficient $\Delta_{ab,N}^{\mathrm{LO}}$ with its resummed analogue $\Delta_{ab,N}^{\mathrm{Res.}}$ [88–90]. Thus, the threshold-resummed $pp \to W_R$ cross section in Mellin space is

$$\sigma_N^{\mathrm{Res.}} = \sigma_0 \mathcal{L}_{q\bar{q}',(N+1)} \times \Delta_{q\bar{q}',(N+1)}^{\mathrm{Res.}}, \tag{43}$$

and in momentum space by the Mellin inverse of the above with respect to τ_0:

$$\sigma^{\mathrm{Res.}}(pp \to W_R + X) = \frac{\sigma_0}{2\pi i} \int_{c-i\infty}^{c+i\infty} dN \tau_0^{-N} \times \mathcal{L}_{q\bar{q}',(N+1)} \times \Delta_{q\bar{q}',(N+1)}^{\mathrm{Res.}}. \tag{44}$$

We approximate the luminosity function $\mathcal{L}(\tau)$ using the Chebyshev polynomial approximation [92,94], which can be Mellin-transformed analytically, and we choose the integration path according to the minimal prescription (MP) procedure [91]. See Appendix A for more details.

Matching resummed and FO calculations beyond LO requires subtracting the soft contributions common to both calculations to avoid phase-space double counting. For a FO result at $\mathrm{N}^k\mathrm{LO}$, this can be done by Taylor-expanding $\sigma^{\mathrm{Res.}}$ up to $\mathcal{O}(\alpha_s^k)$, subtracting these terms from $\sigma^{\mathrm{Res.}}$, and adding the $\mathrm{N}^k\mathrm{LO}$ calculation to the residual resummed expression. One may interpret this procedure as augmenting with approximate $\mathcal{O}(\alpha_s^k)$ terms in $\sigma^{\mathrm{Res.}}$, i.e., soft or nonhard, with the full $\mathcal{O}(\alpha_s^k)$ calculation, which accurately describes both soft and hard radiation. Subsequently, W_R production matched at $\mathrm{N}^k\mathrm{LO} + \mathrm{N}^j\mathrm{LL}$ is given by

$$\sigma^{\mathrm{N}^k\mathrm{LO}+\mathrm{N}^j\mathrm{LL}}(pp \to W_R + X) = \sigma^{\mathrm{N}^k\mathrm{LO}} + \sigma^{\mathrm{N}^j\mathrm{LL}} - \sum_{l=0}^{k} \frac{\alpha_s^l}{l!} \left[\frac{d^l}{d\alpha_s^l}\sigma^{\mathrm{N}^j\mathrm{LL}}\right]_{\alpha_s=0}. \quad (45)$$

In Fig. 3, we show the total inclusive $pp \to W_R$ cross section at NLO + NNLL (dashed-dotted) with PDF uncertainty (shaded), NLO (dashed), and LO (solid) at (a) 13 and (b) 100 TeV. The production rates at 13 (100) TeV span approximately

$$2\ \text{fb–}40\ \text{pb}(90\ \text{ab–}930\ \text{pb}) \quad \text{for } M_{W_R} = 1\text{–}5(1\text{–}33)\ \text{TeV}. \quad (46)$$

In the lower panel are the NLO + NNLL and NLO K-factors, defined respectively as

$$K^{\mathrm{NLO+NNLL}} \equiv \frac{\sigma^{\mathrm{NLO+NNLL}}}{\sigma^{\mathrm{LO}}} \quad \text{and} \quad K^{\mathrm{NLO}} \equiv \frac{\sigma^{\mathrm{NLO}}}{\sigma^{\mathrm{LO}}}. \quad (47)$$

The NLO + NNLL (dashed-dotted) and NLO (dashed) K-factors with uncertainties span roughly

$$K^{\mathrm{NLO+NNLL}}\text{: } 1.2\text{–}2.4(1.2\text{–}1.5), \quad (48)$$

$$K^{\mathrm{NLO}}\text{: } 1.2\text{–}1.4(1.1\text{–}1.3). \quad (49)$$

At 13 and 100 TeV, we observe that the effects of resummation become important with respect to the NLO rate at $\tau_0 \approx 0.3$. At 13 TeV, the resummed corrections for $\tau_0 > 0.3$ are very large, increasing the Born (NLO) predictions by 40–140(4–70)% for $M_{W_R} = 4$–5 TeV. The largeness of the 13 TeV K-factors for $M_{W_R} \gtrsim 4$ TeV does not indicate the breakdown of perturbation theory. Rather, it demonstrates the importance of soft radiation as $\tau_0 \to 1$, and is typical for processes near the boundaries of phase space [91]. This is exemplified at 100 TeV by the reduced importance of resummation for comparable M_{W_R} (smaller τ_0). Despite the largeness of the PDF uncertainties at large M_{W_R}, the NLO + NNLL central value remains within the NLO uncertainty, as seen in the lower panel of Fig. 3(a). See Sec. III D for further discussions on uncertainties. Away from threshold, the resummed calculation converges to the FO result, consistent with expectations [69]. For select M_{W_R}, we summarize our NLO and NLO + NNLL results in Table I.

B. W_R decay

As discussed in Secs. II A and II B, $W_R - W_L$ and $N_i - \nu_i$ mixing are negligibly small and $m_{\mathrm{FCNH}} \gg M_{W_R}$.

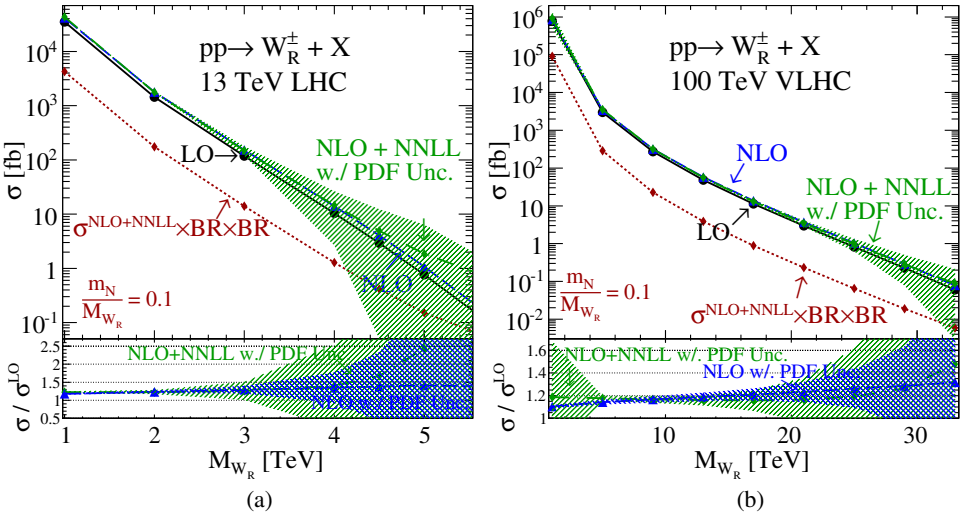

FIG. 3. Upper panel: As a function of M_{W_R}, $pp \to W_R$ production cross section for $\sqrt{s} =$ (a) 13 and (b) 100 TeV, at LO (solid), NLO (dashed), and NLO + NNLL (dashed-dotted) with 1σ PDF uncertainty (shaded), as well as $\sigma^{\mathrm{NLO+NNLL}}(pp \to W_R) \times \mathrm{BR}(W_R \to Ne) \times \mathrm{BR}(N \to eq\bar{q}')$ (dotted). Lower panel: NLO (dashed) and NLO + NNLL (dashed-dotted) K-factors and PDF uncertainties.

TABLE I. The $pp \to W_R$ production cross sections and K-factors at various accuracies for representative M_{W_R} and $\sqrt{s} = 13, 100$ TeV, with absolute scale (first) and PDF (second) uncertainties. Exceptionally small uncertainties are noted by $(< 0.5\%)$.

$\sigma(pp \to W_R^{\pm})$ [fb]					
13 TeV LHC					
M_{W_R}	$\sigma^{\rm LO}$	$\sigma^{\rm NLO}$	$K^{\rm NLO}$	$\sigma^{\rm NLO+NNLL}$	$K^{\rm NLO+}_{\rm NNLL}$
1 TeV	3.52×10^4	$4.15^{+0.08+0.08}_{-0.07-0.08} \times 10^4$	1.18	$4.33^{+(<0.5\%)+0.09}_{-(<0.5\%)-0.09} \times 10^4$	1.23
3 TeV	1.18×10^2	$1.51^{+0.06+0.13}_{-0.06-0.13} \times 10^2$	1.29	$1.48^{+(<0.5\%)+0.3}_{-(<0.5\%)-0.3} \times 10^2$	1.25
5 TeV	0.765	$1.08^{+0.07+1.75}_{-0.07-1.75}$	1.41	$1.86^{+(<0.5\%)+4.55}_{-(<0.5\%)-4.55}$	2.43
100 TeV VLHC					
M_{W_R}	$\sigma^{\rm LO}$	$\sigma^{\rm NLO}$	$K^{\rm NLO}$	$\sigma^{\rm NLO+NNLL}$	$K^{\rm NLO+}_{\rm NNLL}$
1 TeV	7.78×10^5	$8.60^{+0.06+0.09}_{-(<0.5\%)-0.09} \times 10^5$	1.11	$9.25^{+0.23+3.81}_{-0.19-3.81} \times 10^5$	1.19
5 TeV	2.98×10^3	$3.40^{+0.04+0.05}_{-0.03-0.05} \times 10^3$	1.14	$3.50^{+0.02+0.06}_{-(<0.5\%)-0.06} \times 10^3$	1.17
25 TeV	0.818	$1.03^{+0.03+0.14}_{-0.03-0.14}$	1.26	$0.970^{+(<0.5\%)+0.342}_{-(<0.5\%)-0.342}$	1.19
33 TeV	5.98×10^{-2}	$7.86^{+0.31+4.66}_{-0.34-4.66} \times 10^{-2}$	1.31	$8.81^{+(<0.5\%)+12.2}_{-(<0.5\%)-12.2} \times 10^{-2}$	1.47

Subsequently, for $m_N < M_{W_R}$, the only open W_R decay modes are to quark and $\ell^{\pm}N$ pairs. The corresponding partial widths are

$$\Gamma(W_R \to q\bar{q}') = N_c |V^{\rm CKM'}_{qq'}|^2 \frac{g^2 M_{W_R}}{48\pi}, \tag{50}$$

$$\Gamma(W_R \to tb) = N_c |V^{\rm CKM'}_{tb}|^2 \frac{g^2 M_{W_R}}{48\pi} (1 - r_t)^2 \left(1 + \frac{1}{2} r_t\right), \tag{51}$$

$$\Gamma(W_R \to \ell N) = |Y_{\ell N}|^2 \frac{g^2 M_{W_R}}{48\pi} (1 - r_N)^2 \left(1 + \frac{1}{2} r_N\right), \qquad r_i = \frac{m_i^2}{M_{W_R}^2}. \tag{52}$$

For our choice of quark and lepton mixing, the total W_R width is

$$\Gamma_{W_R} = 2\Gamma(W_R \to q\bar{q}') + \Gamma(W_R \to tb) + \Gamma(W_R \to eN) \tag{53}$$

$$= \frac{g^2 M_{W_R}}{48\pi} \left[2N_c + N_c (1 - r_t)^2 \left(1 + \frac{1}{2} r_t\right) + (1 - r_N)^2 \left(1 + \frac{1}{2} r_N\right)\right]. \tag{54}$$

We calculate the total W_R and N decay widths for representative masses in Table II.

The branching fraction of A to final-state X_i is defined as

$$\mathrm{BR}(A \to X_i) \equiv \frac{\Gamma(A \to X_i)}{\sum_i \Gamma(A \to X_i)}. \tag{55}$$

In the large M_{W_R} limit, the W_R branching fractions converge to the asymptotic values

$$\mathrm{BR}(W_R \to q\bar{q}') \approx 2 \times \mathrm{BR}(W_R \to tb) \approx \frac{2N_c}{3N_c + 1} = 60\%, \tag{56}$$

$$\mathrm{BR}(W_R \to Ne) \approx \frac{1}{3N_c + 1} = 10\%. \tag{57}$$

In the upper (lower) panel of Fig. 4(a), we show the total W_R decay width (branching fraction) for $M_{W_R} > 1$ TeV and fixed m_N/M_{W_R} ratios of $\sqrt{r_N} = 0.01$ (dashed), 0.1 (solid), 0.5 (dotted), and 0.75 (dotted-dashed). Similar to the EW gauge bosons, the W_R in this model has a narrow width for all values of M_{W_R}, with Γ_{W_R}/M_{W_R} scaling as

$$\frac{\Gamma_{W_R}}{M_{W_R}} \sim \frac{g^2}{48\pi}(3N_c + 1) \approx 2.8\%. \tag{58}$$

This justifies the use of the narrow width approximation (NWA). Furthermore, as $pp \to W_R$ is a DY process, its factorization properties imply that the NLO and NLO + NNLL corrections to its on-shell production and decay to N are equivalent to the production-only corrections, i.e.,

$$\sigma^{\rm NLO(+NNLL)}(pp \to W_R \to e^{\pm}N) \approx \sigma^{\rm NLO(+NNLL)}(pp \to W_R) \times \mathrm{BR}(W_R \to e^{\pm}N). \tag{59}$$

In the lower panel of Fig. 4(a), we observe that the W_R branching fractions remain virtually independent of

TABLE II. Total W_R and N decay widths for representative M_{W_R} and m_N.

(M_{W_R}, m_N) [TeV, GeV]	(3, 30)	(3, 150)	(3, 300)	(4, 400)	(5, 500)
Γ_{W_R} [GeV]	84.4	84.3	84.2	112	141
Γ_N [eV]	3.41×10^{-3}	10.7	355	513	687

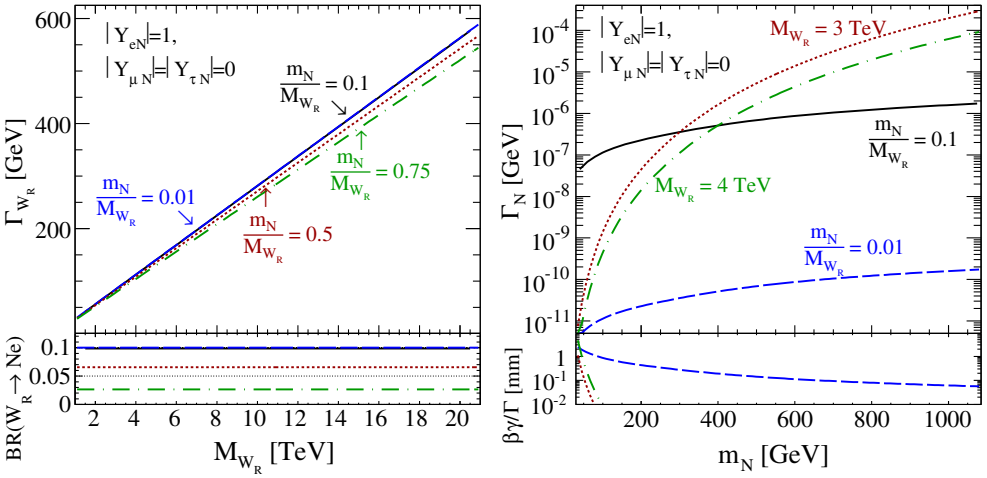

FIG. 4. Total decay widths for representative $\sqrt{r_N} = m_N/M_{W_R}$ of (a) W_R as a function of M_{W_R} and (b) N as a function of m_N. Lower: (a) $W_R \to Ne$ branching fraction; (b) N mean lifetime $d = \beta\gamma/\Gamma_N$ in W_R frame [mm].

m_N and attain its maximum branching of $\mathrm{BR}(W_R \to Ne^{\pm}) \approx 0.1$. For 13 (100) TeV and $(m_N/M_{W_R}) = 0.1$, the $pp \to W_R \to Ne$ cross section [Eq. (59)] spans

$$180\ \text{pb}–15\ \text{fb}(100\ \text{pb}–350\ \text{fb}) \quad \text{for } M_{W_R} = 3–5(5–25)\ \text{TeV}. \tag{60}$$

For representative (M_{W_R}, m_N), we summarize our results in column 2 of Table III.

C. N decays

In our scenario, the heavy neutrino dominantly decays to the three-body final state

$$N \to e^{\pm} W_R^{\mp *} \to e^{\pm} q\bar{q}'. \tag{61}$$

TABLE III. Cross section times branching ratio predictions for $pp \to W_R^{\pm} \to Ne^{\pm}$, with subsequent decay of N to leptons and quarks, for select (M_{W_R}, m_N).

13 TeV LHC [fb]		
(M_{W_R}, m_N) [TeV, GeV]	$\sigma^{\mathrm{NLO+NNLL}} \times \mathrm{BR}(W_R \to Ne)$	$\times \mathrm{BR}(N \to e^{\pm} q\bar{q}')$
(3, 30)	14.8	14.8
(3, 150)	14.8	14.8
(3, 300)	14.6	14.1
(4, 400)	1.44	1.28
(5, 500)	0.184	0.152
100 TeV VLHC [fb]		
(M_{W_R}, m_N) [TeV, GeV]	$\sigma^{\mathrm{NLO+NNLL}} \times \mathrm{BR}(W_R \to Ne)$	$\times \mathrm{BR}(N \to e^{\pm} q\bar{q}')$
(5, 500)	345	286
(25, 2500)	95.7×10^{-3}	64.6×10^{-3}

Both e^+ and e^- are allowed in the final state due to the Majorana nature of N. If kinematically accessible, the heavy neutrino can also decay to t and b quarks, with the final state $e^{\pm}tb$. In principle, N can also decay to SM EW bosons via mixing with SM neutrinos; the rate is controlled by the tiny mixing parameter $|X_{\ell N}|^2 \sim 1 - |Y_{\ell N}|^2 \sim \mathcal{O}(m_\nu^2/m_N^2)$. Following Eq. (27), such decays vanish at tree level and, therefore, are not considered in the analysis. For $m_N \ll M_{W_R}$, the partial widths of N are

$$\Gamma(N \to e^{\pm} q\bar{q}') = 2N_c \frac{|Y_{\ell N}|^2 |V_{qq'}^{\mathrm{CKM}'}|^2 g^4 m_N^5}{3 \cdot 2^{11} \cdot \pi^3 M_{W_R}^4},$$
$$y_t = \frac{m_t^2}{m_N^2}, \tag{62}$$

$$\Gamma(N \to e^{\pm} tb) = 2N_c \frac{|Y_{\ell N}|^2 |V_{tb}^{\mathrm{CKM}'}|^2 g^4 m_N^5}{3 \cdot 2^{11} \cdot \pi^3 M_{W_R}^4} \times (1 - 8y_t + 8y_t^3 - y_t^4 - 12y_t^2 \log y_t). \tag{63}$$

The validity of this approximation for $m_N/M_{W_R} \sim 0.1$ has been checked against MG5. For our choice of mixing, the total N width is

$$\Gamma_N = 2\Gamma(N \to e^{\pm} q\bar{q}') + \Gamma(N \to e^{\pm} tb) \tag{64}$$

$$= 2N_c \frac{g^4 m_N^5}{3 \cdot 2^{11} \cdot \pi^3 M_{W_R}^4} [3 - 8y_t + 8y_t^3 - y_t^4 - 12y_t^2 \log y_t] \tag{65}$$

and implies that Γ_N/m_N scales as

$$\frac{\Gamma_N}{m_N} = \frac{g^4}{2^{10}\pi^3}\left(\frac{m_N}{M_{W_R}}\right)^4 \sim 5\times 10^{-6}\times\left(\frac{m_N}{M_{W_R}}\right)^4 \ll 1. \quad (66)$$

Hence, application of the NWA in N decays is justified but suggests N may be long-lived. Values of Γ_N for representative M_{W_R} and m_N used in this study are given in Table II.

In Fig. 4(b), we plot Γ_N as a function of m_N for representative M_{W_R} and (m_N/M_{W_R}) ratios; in the lower panel we show the mean flight distances

$$d_0 = v\tau_0 = \beta\gamma\hbar c/\Gamma_N, \qquad \beta\gamma = \frac{(1-r_N)}{2\sqrt{r_N}}. \quad (67)$$

For $m_N = 30$–1000 GeV, we find

$$\frac{m_N}{M_{W_R}} = 0.1(\text{solid}):\ \Gamma_N \sim 10^{-8}\text{–}10^{-6}\ \text{GeV}, \quad (68)$$

$$\frac{m_N}{M_{W_R}} = 0.01(\text{dashed}):\ \Gamma_N \sim 10^{-12}\text{–}10^{-10}\ \text{GeV}. \quad (69)$$

The corresponding mean flight distances span

$$\frac{m_N}{M_{W_R}} = 0.1(\text{solid}):\ d_0 \sim 10^{-7}\text{–}10^{-5}\ \text{mm}, \quad (70)$$

$$\frac{m_N}{M_{W_R}} = 0.01(\text{dashed}):\ d_0 \sim 10^{-2}\text{–}3\ \text{mm}. \quad (71)$$

This implies that for N much lighter than M_{W_R}, i.e., $m_N/M_{W_R} < 0.01$, heavy neutrinos appear in detector experiments as displaced vertices, not prompt decays. However, such a scenario is not reasonable within the spirit of the LRSM model. Supposing $m_N/M_{W_R} < 0.01$ and using expressions for m_N, M_{W_R} in Secs. II B and II A, the Yukawa couplings of the heavy neutrino N to the triplet Higgs are restricted to $f_R < 3\times 10^{-3}$. This is comparable to generation I and II quark SM Yukawa couplings. However, taking $m_N \sim \mathcal{O}(10)$ GeV, a (vanilla) type I seesaw model then requires, for light neutrino masses $m_{\nu_m} \sim 0.1$ eV, a Dirac neutrino mass of $m_D \sim 30$ KeV, or a Yukawa coupling $\mathcal{O}(15$–$20)\times$ smaller than the SM electron Yukawa. Though not forbidden, this is contrary to the seesaw model spirit of explaining light neutrino masses without excessively small couplings.

From Eq. (65) the N branching fractions are independent of M_{W_R} and are given by

$$\text{BR}(N\to e^\pm q\bar{q}') = \begin{cases} 1, & m_N \le m_t, \\ \frac{2}{3-8y_t+8y_t^3-y_t^4-12y_t^2\log y_t}, & m_N > m_t, \end{cases} \quad (72)$$

$$\text{BR}(N\to e^\pm tb) = \frac{1-8y_t+8y_t^3-y_t^4-12y_t^2\log y_t}{3-8y_t+8y_t^3-y_t^4-12y_t^2\log y_t}, \quad m_N > m_t. \quad (73)$$

For $M_{W_R} \gg m_N \gg m_t$, one finds asymptotically

$$\text{BR}(N\to e^\pm q\bar{q}') \approx 2\times\text{BR}(N\to e^\pm tb) \approx \frac{2}{3}. \quad (74)$$

Consequently, the 13 and 100 TeV cross sections for the process

$$pp\to W_R\to Ne\to eeq\bar{q}' \quad (75)$$

in the NWA approximation can be given in terms of Eq. (59):

$$\sigma^{\text{NLO(+NNLL)}}(pp\to W_R^\pm\to Ne^\pm\to e^\pm e^\pm q\bar{q}') \approx \sigma^{\text{NLO(+NNLL)}}(pp\to W_R^\pm)\times\text{BR}(W_R\to Ne)\text{BR}(N\to e^\pm q\bar{q}'). \quad (76)$$

The total production rates for Eq. (76) for representative (M_{W_R}, m_N) are summarized in column 3 of Table III and for $m_N/M_{W_R} = 0.1$ plotted in Fig. 3 (dotted). We find that the total 13 (100) TeV rate spans approximately

$$10^{-1}\text{–}4\times 10^4(10^{-3}\text{–}10^5)\ \text{fb} \quad \text{for } M_{W_R} = 1\text{–}5(35)\ \text{TeV}. \quad (77)$$

D. PDF and scale uncertainties

To estimate the impact of higher order terms in the QCD perturbative series that are not calculated in the W_R production cross section, we vary the factorization and renormalization scales about the default choice of $\mu_0 = M_{W_R}$ up and down by a factor of 2. We present results normalized to the cross section at the default scale. In the lower panel of each plot is the K-factor as defined in Eq. (47).

In Fig. 5 we show the effect of scale variation on the NLO cross section at (a) 13 and (b) 100 TeV for a range of W_R masses. At NLO, it can be seen at both 13 and 100 TeV that increasing (decreasing) the default scale lowers (raises) the total cross section, except for very low W_R masses at 100 TeV, a feature common to high-mass DY processes [86]. In addition, the K-factor also steadily increases with mass, indicating the growing importance of higher order corrections in such scenarios. In both the 13 and 100 TeV cases, the scale variation results in a 2%–5% uncertainty to the total cross section.

The effect of scale variations on the NLO + NNLL result is presented at (c) 13 and (d) 100 TeV for the same M_{W_R}. The effect of the resummation on the scale variation is manifest in the reduction of the associated uncertainty. For the 13 TeV case, uncertainty is reduced to the subpercent level, while at 100 TeV the impact is comparable to (but smaller than) the NLO dependence. This is because resummed contributions are less important away from threshold. Indeed, the observed reduction in scale

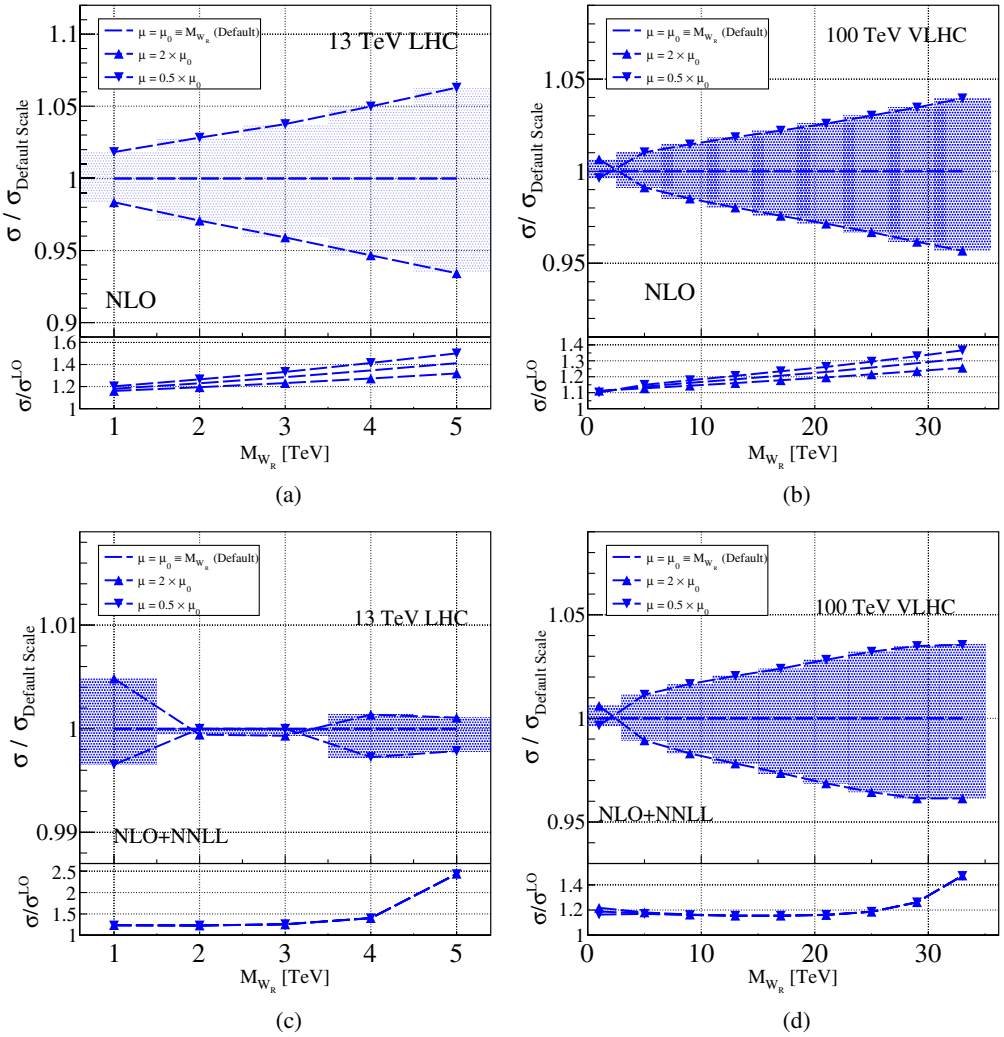

FIG. 5. Scale dependence of the total W_R cross section and associated K-factors at NLO for (a) 13 and (b) 100 TeV, and NLO + NNLL for (c) 13 and (d) 100 TeV.

uncertainty is consistent with what one expects from including higher order terms in the perturbative series.

We calculate the symmetric PDF uncertainties from the NNPDF member sets following the recommended procedure of Ref. [79]. The 68% (1σ) uncertainty bands are represented by the shaded regions in Fig. 3. In the upper panel, only the NLO + NNLL uncertainties are shown; in the lower panel, both the NLO and NLO + NNLL uncertainties are shown. At 13 TeV, for $M_{W_R} = 4(4.5)$ TeV, the NLO + NNLL uncertainty is approximately $\pm 80(240)\%$. At 100 TeV, the uncertainties breach 100% for M_{W_R} between 20 and 30 TeV.

The larger uncertainties in the threshold calculation compared to the NLO result are due in part to less data being used to constrain the threshold-improved PDFs [69,70]. This follows from the limited threshold calculations available for processes that enter into global fit PDFs, and it demonstrates their need for accurate LHC predictions.

For representative M_{W_R}, scale and PDF uncertainties are given in Table I.

IV. OBSERVABILITY OF BOOSTED N AT HADRON COLLIDERS

In this section we study the observability at hadron colliders of W_R and N in the LRSM for $m_N/M_{W_R} \lesssim 0.1$. We start with production- and decay-level kinematics of N at LO. After constructing several observables with strong background-discriminating power, we perform a full parton shower (PS)/detector-level signal-to-background analysis.

For signal event generation, we modify the Manifest LRSM FeynRules (FR) model file v1.1.6_mix by Ref. [73] (see Appendix B 2) and use FR v2.3.10 [95,96] to generate universal file object (UFO) inputs [97]. LO events are simulated using MG5 [87]. Rates are scaled by the NLO + NNLL K-factors as defined in Eq. (47). Application of K-factors is justified in the threshold regime as the dominant

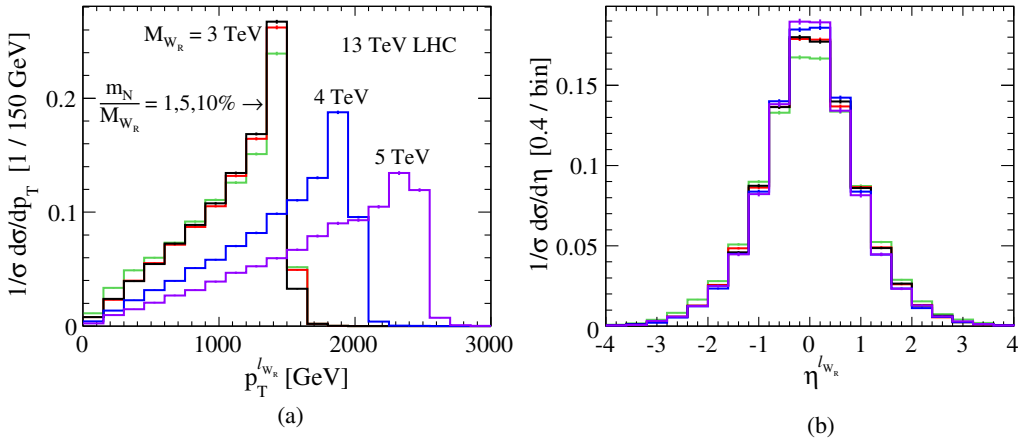

FIG. 6. Normalized (a) transverse momentum (p_T) and (b) pseudorapidity (η) distributions of the charged lepton from $pp \to W_R \to N\ell$ for representative M_{W_R} and m_N at 13 TeV.

contribution, i.e., soft-radiation, largely leave kinematics unchanged. Events are showered using PYTHIA 8.212 [98], and jets are clustered with FastJet v3.20 [99,100] using the Cambridge/Aachen (C/A) algorithm [101,102] with a separation parameter of $R = 1.0$. SM background processes are simulated at LO + PS accuracy using the MG5 and are scaled by an appropriate NLO K-factor calculated via the MG5_aMC@NLO framework. Due to extreme phase-space cuts, event generation at NLO + PS accuracy is impractical.

A. Kinematic properties of boosted N

To investigate the kinematics of boosted N from W_R decays, we simulate at 13 TeV

$$q_1\bar{q}_2 \to W_R \to e_1 N \to e_1 e_2 q_1' \bar{q}_2', \tag{78}$$

where the two electrons possess any electric charge combination, for the representative (M_{W_R}, m_N) listed in Table II. We focus on final-state electrons, which is the most problematic channel for ATLAS and CMS [54,55], but our study is also applicable to the $e\mu$ and $\mu\mu$ final states. The largest change in those channels follows from the better muon identification compared to the electron [62]; this in fact extends the validity of standard dilepton searches. Inclusion of the $N \to \ell tb$ final state is similarly straightforward. To model detector response while keeping generator-level particle identification at LO, we smear final-state partons as done in [103], which adopts the expected ATLAS detector performance parametrization [104]. Equation (78) is free of kinematic poles, and no generator-level cuts are applied.

In Fig. 6 we show the normalized differential distributions with respect to the (a) transverse momentum (p_T) and (b) pseudorapidity (η) of the charged lepton in the $W_R^\pm \to Ne^\pm$ decay, denoted by ℓ_{W_R}. In the $p_T^{\ell_{W_R}}$ distribution, the Jacobian peak near $p_T \sim M_{W_R}/2$ is unambiguous and is largely independent of such small m_N. The $\eta^{\ell_{W_R}}$ distribution reveals that ℓ_{W_R} are very central, with most electrons contained within $|\eta| < 1.0$ and negligibly few with $|\eta| \geq 2.0$. Multi-TeV bounds on M_{W_R} (see Sec. II) nearly guarantee that $p_T^{\ell_{W_R}}$ is very large and $|\eta^\ell|$ small. Consequently, Eq. (78) efficiently passes inclusive high-p_T single-electron triggers, such as those used in Ref. [62].

As $pp \to Ne^\pm$ is a $2 \to 2$ system, the heavy neutrino's p_T and rapidity (y) distributions are identical to Fig. 6, up to mass corrections. Hence, the decay products of the N with high p_T are largely collimated due to its relative lightness. For the $N \to \ell_N q\bar{q}'$ final state in Eq. (78), we show in Fig. 7 the normalized separation[1] distributions between (a) the charged lepton ℓ_N and its closest quark ($\Delta R^{\min}_{q\ell_N}$), as well as (b) the two quarks themselves ($\Delta R_{q\bar{q}'}$). In both cases, the separation peaks at $\Delta R \sim 0.2(0.4)$ for $\sqrt{r_N} = m_N/M_{W_R} = 0.05(0.1)$, and follows from the scaling relationship

$$\Delta R_{qX} \sim 2p_\perp^X/p_T^N \sim 4m_N/M_{W_R}, \tag{79}$$

where $p_\perp^X$ is the perpendicular momentum of $X = \ell_N, \bar{q}'$ relative to its parent N. Hence, for much of the phase space, these electrons fail particle identification criteria at 13 TeV [62]:

$$p_T^\ell > 35 \text{ GeV}, \qquad \Delta R_{\ell X} > 0.3, \qquad |\eta^\ell| < 2.4, \tag{80}$$

and this leads to the breakdown of current ATLAS and CMS $W_R - N$ search strategies [54]. Smaller $r_N = m_N^2/M_{W_R}^2$, hadronization, and the presence of tb pairs exacerbate this issue.

[1]The separation between particle pair (a, b) is defined as $\Delta R_{ab} \equiv \sqrt{(y_a - y_b)^2 + (\phi_a - \phi_b)^2}$ for rapidity y (or pseudorapidity η) and azimuthal angle ϕ.

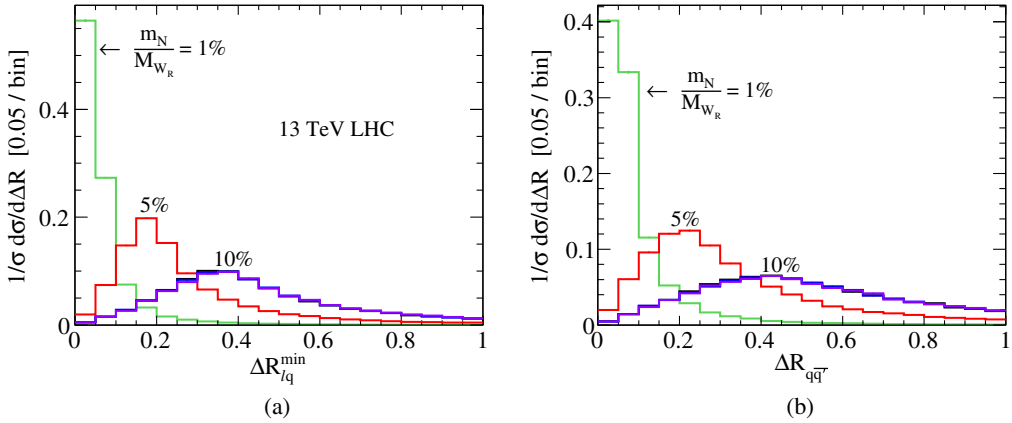

FIG. 7. Normalized distributions with respect to (a) $\Delta R_{\ell q}^{\min}$ and (b) $\Delta R_{q\bar{q}'}$ of N decay products for same configuration as in Fig. 6.

For such signal regions, we consider an alternate search strategy: model the N decay products as a single object, which we call a neutrino jet (j_N), and investigate instead the $2 \to 2$ process:

$$pp \to W_R \to e^{\pm} j_N. \tag{81}$$

The simplified signal topology alleviates the failing identification criteria and retains the high signal-to-noise properties of the same-sign dilepton channel. To build a qualitative picture of the new signal definition, we preliminarily define j_N at the present FO parton level via C/A clustering with $\Delta R = 1$. We cluster all final-state partons except any electron candidate satisfying Eq. (80). Note that j_N is identified as the highest p_T C/A jet.

In Fig. 8 we show the normalized distributions for j_N with respect to (a) p_T, (b) y, (c) invariant mass (m_{j_N}), and (d) missing transverse momentum (MET) for events with

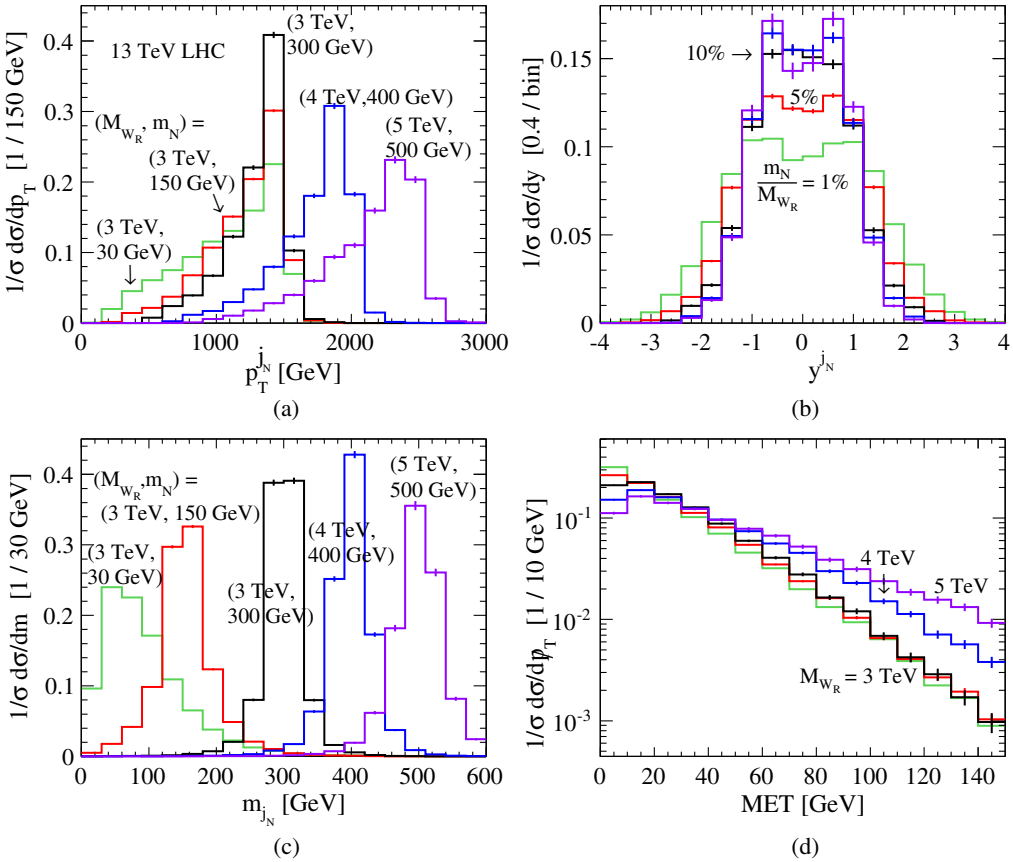

FIG. 8. Normalized distributions with respect to (a) $p_T^{j_N}$, (b) y^{j_N}, (c) m_{j_N}, and (d) MET for the same configuration as in Fig. 6 but requiring exactly one electron and one j_N candidate.

exactly one electron and one j_N candidate. As anticipated, we observe strong similarities to the ℓ_{W_R} distributions and unambiguous Breit-Wigner resonances at the appropriate values in the m_{j_N} distribution. This indicates that j_N is a good description of N and that the signal definition of Eq. (81) can be interpreted as Eq. (78) when $(m_N/M_{W_R}) < 0.1$.

A cost of this new signal definition is the loss of the unambiguous smoking-gun collider signature of two same-sign leptons and jets [37], which is intrinsically background-free up to detector effects as it violates L by two units. However, inherited from the original definition is the fact that, up to detector and hadronization effects, the process has no MET as no light neutrinos exist in the final state. Requiring again exactly one electron candidate, we show in (d) the normalized MET distribution. Due to smearing, we find moderate MET out to $10s$ of GeV and largely independent of m_N. We observe that the peak MET shifts to larger values for larger M_{W_R}, and this is due to the increased likelihood of more energy being misreconstructed for more energetic objects [104]. Present ATLAS detector capabilities [105] permit MET cuts as tight as

$$\text{MET} < 35 \text{ GeV}. \tag{82}$$

In a realistic scenario (see Sec. IV B), a more conservative cut is required due to pileup, etc.

In Fig. 9(a) the W_R resonances built from the $\ell_1 - j_N$ invariant mass are clearly seen for our representative masses, up to broadening due to misreconstruction of N and detector smearing. In (b), we show the polarization of ℓ_1 in the $\ell_1 - j_N$ system's rest frame. We clearly observe the RH chiral structure of the $N\ell W_R$ vertex for $\sqrt{r_N} = m_N/M_{W_R} = 0.01$. At larger r_N, however, this becomes obfuscated due to the importance of opposite helicity states, which scale like r_N, and lead to spin decorrelation.

Altogether, this demonstrates the viability of the new search procedure.

Aside from the application of microjets and substructure techniques, it may be possible to verify the Majorana nature of heavier N via its decays to top quarks. For Dirac N, the off-shell W_R^* to which it decays can only carry the same electric charge as the charged lepton produced from the decay of the primary, on-shell W_R, i.e., ℓ_{W_R}. Decays of the W_R^* to a top quark that subsequently decays leptonically can lead to final-state muons with the *same* sign electric charge as ℓ_{W_R}. That is, for a fixed primary W_R electric charge, one has

$$\begin{aligned} q\bar{q}' \to W_R^{\pm} \to \ell_{W_R}^{\pm} N, \quad \text{with} \\ N \to \ell_N^{\mp}(t \to W_L^{\pm} b) b \to \ell_N^{\mp} b\bar{b}\mu^{\pm}\nu_{\mu}. \end{aligned} \tag{83}$$

Hence, j_N containing top quarks can be identified by their larger complexity, namely, the presence of two b subjets. As the outgoing muon momentum scales like $p_T^{\mu} \sim \gamma_t m_t(1 + M_W^2/m_t^2)/4 \sim \gamma_t 50$ GeV, where $\gamma_t \sim m_t/p_T^N \sim m_t/M_{W_R}$ is the top quark's Lorentz boost to the lab frame, it should be identifiable. For a Majorana N, the off-shell W_R^* can carry either electric charge. Thus, observation of such muons with *opposite* electric charge of the easily identifiable ℓ_{W_R} is evidence of L-violating transitions. Further discussion of this topic is beyond the scope of this study.

We briefly note that the use of neutrino jets is also widely applicable to other situations: In the MLRSM, high-mass Z_R and H_{FCNH} decays to boosted NN pairs could give rise to two back-to-back j_N. If N couples non-negligibly to EW bosons, then j_N may also feature substructure topologies. In other models, such as the inverse seesaw model, rare decays of $W/Z/h$ bosons to GeV-scale pseudo-Dirac neutrinos, as well as other processes, could also result in j_N.

1. Estimation of leading standard model backgrounds

Before simulating our full detector-level analysis, we are in the position to estimate the leading SM backgrounds. The simple lepton + jet topology of Eq. (81) suffers from large SM backgrounds. We sort the leading channels into

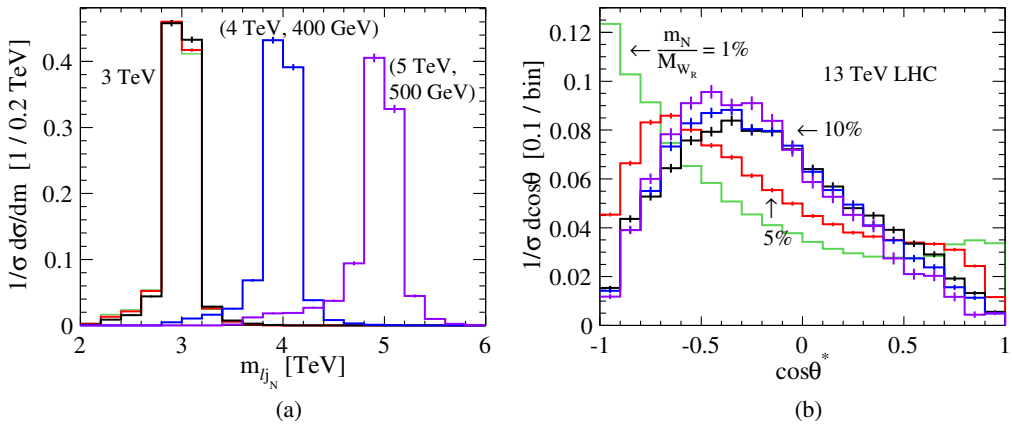

FIG. 9. (a) Invariant mass $m_{\ell_1 j_N}$ and (b) polar distribution of ℓ_1 in the $(\ell_1 - j_N)$ system's rest frame for the same configuration as in Fig. 8.

three categories: (a) weak bosons, (b) top quarks, and (c) fake rates from electron misidentification:

$$\text{Weak boson}: W^{\pm}j(\to e^{\pm}jX), \quad W^{\pm}Z(\to e^{\pm}jX), \tag{84}$$

$$\text{Top quark}: t\bar{t}+nj(\text{semileptonic}), \quad tbj(\to \ell^{\pm}+nb+mjX), \tag{85}$$

$$\text{Fake rates} \quad : e^{+}e^{-}j, \qquad W^{+}W^{-}j(\to e^{+}e^{-}jX). \tag{86}$$

Fake events correspond to regions of phase space where one electron candidate is identified according to Eq. (80) but additional electrons fail to pass the criteria.

At the generator level and assuming the following (nominal) regulating cuts,

$$p_T^{j,b} > 30 \text{ GeV}, \qquad \Delta R_{jb} > 0.4, \qquad \Delta R_{\ell X} > 0.3, \qquad |\eta^{j,b}| < 4.5, \tag{87}$$

the DY $+ 1j$ channels at LO, i.e., Wj and eej, are found to dominate with cross sections reaching $\sigma^{\text{SM}} \sim 0.3$–$2$ nb; see row 1 of Table IV. The signal-to-noise ratio roughly translates to $S/N \sim 10^{-6}$–10^{-5}. Background rates are dramatically reduced after decaying the top quark and EW bosons and requiring that the p_T of the leading charged lepton and process MET satisfy, at the generator level,

$$p_T^{\ell_1 \text{Generator level}} > 1 \text{ TeV} \quad \text{and} \quad \text{MET}^{\text{Generator level}} < 50 \text{ GeV}. \tag{88}$$

The Wj and eej channels remain dominant but now only reach $\sigma^{\text{SM}} \sim 200$ ab; see row 2 of Table IV. The top background is particularly neutralized owing to the cascade nature of their decays, which require TeV-scale charged leptons to be accompanied by TeV-scale light neutrinos from a multi-TeV top quark parent. Subsequently, the top quark and diboson backgrounds can be neglected.

Requiring exactly one charged lepton to satisfy the electron identification of Eq. (80) and rejecting events with additional electrons leaves the Wj rate largely unchanged but reduces the neutral current DY background to the $\sigma^{\text{SM}} \sim 60$ ab level; see row 3 of Table IV. Imposing the MET requirement of Eq. (82) after smearing indicates that the remaining SM background sums to a total of $\sigma^{\text{SM}} \sim 110$ ab; see row 4 of Table IV. We calculate a NLO K-factor of $K^{\text{NLO}} = 1.30$ for the Wj channel; the same K-factor is applicable to the eej channel due to color symmetry. This increases the total SM background to $\sigma^{\text{SM}} \sim 140$–$150$ ab; see row 5 of Table IV. After incorporating a loose $m_{\ell j_{\text{Fat}}}$ cut around M_{W_R} and an appropriate signal K-factor, the signal-to-noise ratio exceeds $S/N \gtrsim 10$–100.

B. Detector-level signal analysis and neutrino jet definition

Using a custom detector simulation, we model the effects of detector resolution and efficiency based closely on the ATLAS Kraków parametrization [106]. The parametrization provides a conservative estimate of the ATLAS detector performance for the phase-II high-luminosity LHC. We model pileup (with $\mu = 80$) and ΣE_T-dependent resolutions for jets and MET. We define an electron to be isolated if the hadronic energy deposit within a cone of size $R = 0.3$ is smaller than 10% of the lepton candidate's p_T. For benchmark points we use the (M_{W_R}, m_N) listed in Table II, i.e., $m_N/m_{W_R} \lesssim 0.1$ at $\sqrt{s} = 13$ and 100 TeV. We summarize our analysis in Table V.

As described in Sec. IV A, the angular separation between the charged lepton and the W_R^* decay products in the chain $N \to \ell^{\pm}W^{\mp} \to \ell^{\pm}q\bar{q}'$ depends on the $W_R - N$ mass hierarchy. A significant amount of radiation from the W_R^* decay enters the isolation cone of ℓ and can negatively affect the lepton's identification. While so-called mini-isolation requirements [107] can be applied to recover the unidentified leptons, we adopt a more conservative approach and include the lepton's momentum as part of a fat jet (j_{Fat}), recombined with the C/A algorithm and a cone size of $R = 1.0$, i.e., j_N. Hence, we focus on the inclusive process

$$pp \to W_R \to e^{\pm}N \to e^{\pm}j_{\text{Fat}}. \tag{89}$$

We require the electron and j_{Fat} to further satisfy

$$p_T^{\ell} > 1 \text{ TeV}, \qquad p_T^{j_{\text{Fat}}} > 1 \text{ TeV}, \qquad |\eta^{\ell}| < 2.5, \qquad |y^{\ell}| < 2.5. \tag{90}$$

TABLE IV. Cross sections [ab] of SM background for $pp \to e^{\pm}j_N$ after decays and successive cuts.

Cut \ σ^{LO} [ab]	Wj	WZ	$t\bar{t}$	$t\bar{t}j$	tbj	eej	WWj
$p_T^{j,b} > 30$ GeV, $\lvert\eta^{j,b}\rvert < 4.5 + \Delta R_{jb} > 0.4$, $\Delta R_{\ell X} > 0.3$No decay	2.17×10^9	11.0×10^6	63.8×10^6	44.0×10^6	4.18×10^6	344×10^6	327×10^3
+Decay + $p_T^{\ell\,\max} > 1$ TeV + $\not{E}_T < 50$ GeV	218	2.61	0.201	0.660	0.062	184	0.637
+Smearing + $\lvert\eta^{\ell}\rvert < 2.0 + p_T^{\ell} > 35$ GeV	218	⋯	⋯	⋯	⋯	57	⋯
+2nd $e^{\pm}$ veto							
$E_T < 35$ GeV	85	⋯	⋯	⋯	⋯	25	⋯
$K^{\text{NLO}} = 1.3$	111	⋯	⋯	⋯	⋯	33	⋯

TABLE V. The $pp \to e^{\pm} j_{\rm Fat}$ rates [fb] after successive cuts and QCD normalization, as well as the acceptance rate and statistical significance after all cuts for representative (M_{W_R}, m_N) at $\sqrt{s} = 13$, 100 TeV.

$\sigma(pp \to W_R^{\pm} \to \ell^{\pm} N \to \ell^{\pm} j_N)$ [fb]					
13 TeV LHC					
	(M_{W_R}, m_N) [TeV, GeV]				
Cut	(3, 30)	(3, 150)	(3, 300)	(4, 400)	(5, 500)
Fiducial + Kinematics + Detector + K-factor [Eq. (90)]	6.87	6.76	6.39	0.69	0.06
MET [Eq. (91)]	4.30 (63%)	4.22 (62%)	4.02 (63%)	0.40 (58%)	0.03 (50%)
$m_{\ell j_{\rm Fat}}$ [Eq. (92)]	3.64 (85%)	3.59 (85%)	3.41 (85%)	0.30 (75%)	0.02 (67%)
$\mathcal{A} = \sigma^{\rm Cuts}/\sigma^{\rm Fid+Kin}$	53%	53%	53%	43%	33%
$\frac{S}{\sqrt{S+B}}$ [$\mathcal{L} = 10$ fb^{-1}]	5.9	5.9	5.7	1.7	0.4
$\frac{S}{\sqrt{S+B}}$ [100 fb^{-1}]	19	19	18	5.4	5.7 [2 ab^{-1}]
100 TeV VLHC					
	(M_{W_R}, m_N) [TeV, GeV]				
Cut	(3, 30)	(3, 150)	(3, 300)	(4, 400)	(5, 500)
Fiducial + Kinematics + Detector + K-factor [Eq. (90)]	1020	1010	957	408	183
MET [Eq. (91)]	597 (58%)	591 (58%)	540 (56%)	223 (55%)	93.0 (51%)
$m_{\ell j_{\rm Fat}}$ [Eq. (92)]	483 (81%)	476 (81%)	433 (80%)	164 (73%)	61.2 (66%)
$\mathcal{A} = \sigma^{\rm Cuts}/\sigma^{\rm Fid+Kin}$	47%	47%	45%	40%	33%
$\frac{S}{\sqrt{S+B}}$ [10 fb^{-1}]	68	67	64	40	24

After kinematic and fiducial cuts, we see in row 5 (14) of Table V that the 13 (100) TeV rate for our representative (M_{W_R}, m_N) spans 60 ab–7 fb (0.2–1 pb). Including the detector response shifts the signal MET distribution to larger values than estimated in Sec. IV A. In order to not lose a majority of the events, we loosen the MET cut of Eq. (82) to

$$\text{MET} < 100 \text{ GeV}. \tag{91}$$

In rows 6 and 15 of Table V, we find that about 50%–60% of events survive the MET requirement, with heavier (lighter) W_R having a lower (higher) survival likelihood. This behavior is due to the increase in momentum mismeasurement at larger p_T scales, which necessarily occurs with heavier M_{W_R}, and is visible in the MET distribution of Fig. 8(d). Similarly, higher collider energies lead to additional secondary radiation and larger MET.

In Fig. 10 we show the invariant mass distributions at LO + PS for the reconstructed heavy neutrino $N = j_{\rm Fat}$ and $W_R = (\ell^{\pm} + j_{\rm Fat})$ systems. The signal is overlaid with the dominant SM $W + 1j$ background, also at LO + PS. At this more realistic level, we find that $j_{\rm Fat}$ indeed still recovers the desired distributions, indicating that neutrino jets are indeed good descriptors of boosted heavy neutrinos, and this further validates our approach.

To further reduce the SM background, we apply the following cut around $m_{\ell j_{\rm Fat}}$:

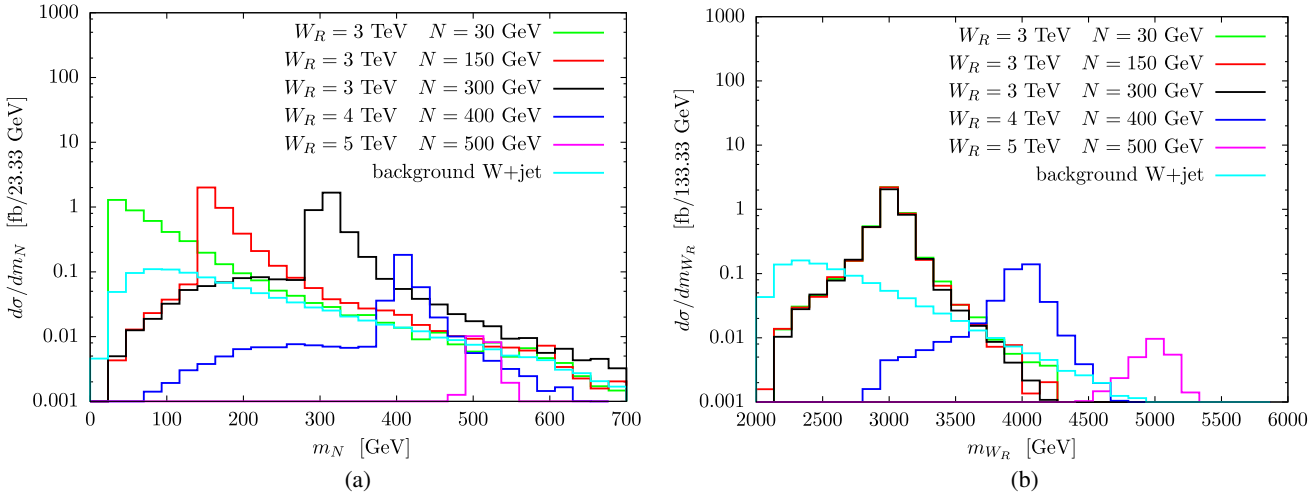

FIG. 10. Mass of the reconstructed (a) neutrino N and (b) W_R including detector effects at LO + PS, as detailed in Sec. IV B.

$$|m_{\ell j_{\rm Fat}} - M_{W_R}| < 200 \text{ GeV}. \quad (92)$$

The largeness of the mass window is motivated by the size of the W_R total width Γ_{W_R}. In row 7 (16) of Table V, we see that roughly 60%–85% (65%–80%) of events at 13 (100) TeV rate pass this cut, again with heavier (lighter) W_R having a lower (higher) survival likelihood. The behavior here can be understood by comparing the 200 GeV mass window to Γ_{W_R} in Table II. For heavier (lighter) W_R, we see that the mass window is about $1.4(2.4) \times \Gamma_{W_R}$, hence encapsulating fewer (more) W_R. As in the parton-level analysis, we find that the residual SM background is negligible.

For 13 (100 TeV) we calculate in row 8 (17) the acceptance rate, defined as the ratio of rows 7 and 5 (16 and 14):

$$\mathcal{A} \equiv \frac{\sigma^{\text{All Cuts}}}{\sigma^{\text{Fiducial+Kinematics+DetectorResponse}}}. \quad (93)$$

We find that approximately 33%–50% of the events pass our selection criteria.

Using the Gaussian estimator,

$$\sigma = \frac{S}{\sqrt{S+B}} \approx \sqrt{S}, \quad \text{for } S(B) = \mathcal{L} \times \sigma^{\text{All Cuts}}_{\text{Signal(SMbackground)}}, \quad (94)$$

we can determine the statistical significance of the signal process (S) over the SM backgrounds (B) after an integrated luminosity of $\mathcal{L}$. At 13 TeV, we find a $> 5\sigma$ statistical observation (discovery) for $M_{W_R} = 3(4)[5]$ TeV, independent of m_N, after $\mathcal{L} = 10(100)[2000]$ fb^{-1}. At 100 TeV and $\mathcal{L} = 10$ fb^{-1}, all benchmark points are in excess of 20σ. This is summarized in rows 9, 10, and 18 of Table V and Figs. 11(a) and 11(b). We extrapolate the discovery potential for higher M_{W_R} by keeping fixed the efficiency, $\varepsilon \equiv \sigma^{\text{Fid+Kin}}/\sigma^{\text{Total}}$, and the acceptance for $(M_{W_R}, m_N) = (5\text{ TeV}, 500\text{ GeV})$, in which case $(\varepsilon \approx 0.64, \mathcal{A} \approx 0.33)$. As seen in Fig. 11(b), a 5σ discovery can be obtained for W_R masses up to $M_{W_R} = 15(30)$ with approximately 100 fb^{-1} (10 ab^{-1}).

Finally, we discuss briefly the 13 and 100 TeV potential to exclude previously unconstrained regions of the (M_{W_R}, m_N) parameter space. We use Poisson counting to deduce the required luminosity $\mathcal{L}_{95}$ for a 95% C.L. exclusion: For a SM

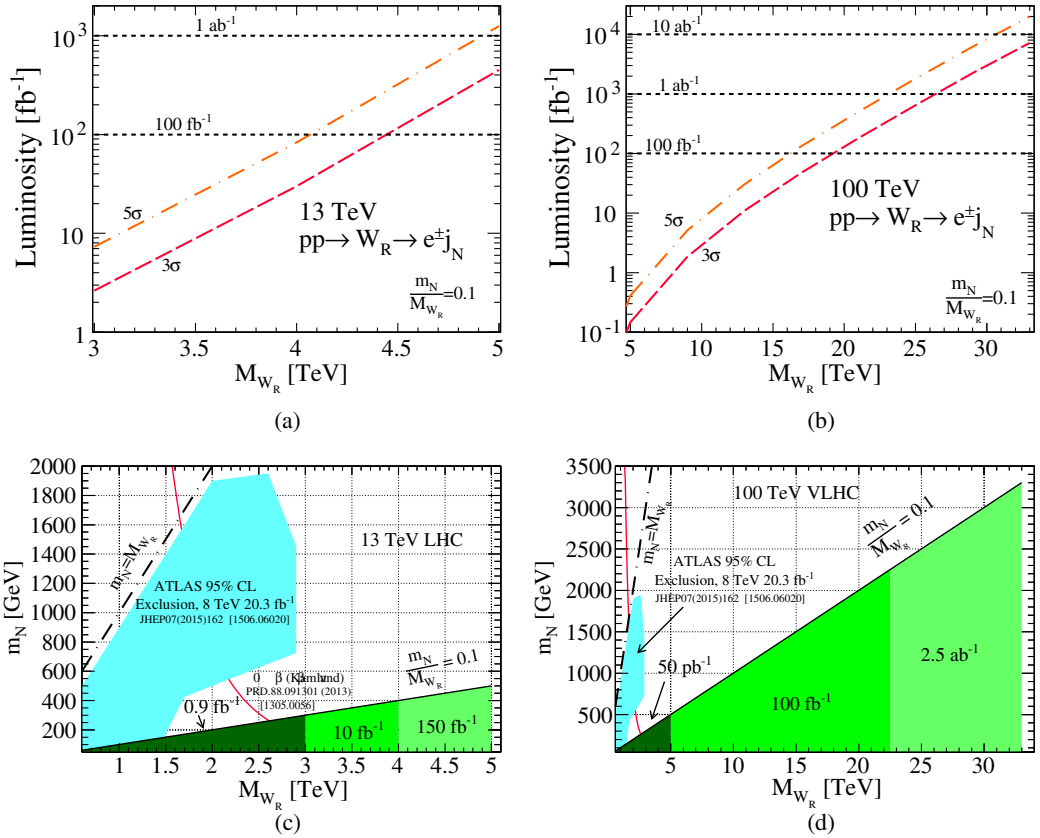

FIG. 11. Discovery (a, b) and 95% CL exclusion (c,d) potential of $pp \to W_R \to e^{\pm} j_N$ searches at (a, c) $\sqrt{s} = 13$ and (b, d) 100 TeV. Also shown in (c, d), ATLAS experiment's 8 TeV 95% CL [54] and KamLAND-Zen 90% CL [31,77] exclusion limits.

background of $B \approx 0$ events, we solve for the largest number of signal events S such that the expected probability to observe B events is at most $5\%(= 1 - \text{C.L.})$; i.e., we find S such that we satisfy

$$\Pr\left(n_{\text{observed}} = B | n_{\text{expected}} = S + B\right) = \frac{(S+B)^B}{B!} e^{-(S+B)} \leq 1 - \text{C.L.} = 0.05. \quad (95)$$

For $B \approx 0$, this yields $S = 3$. Given an efficiency ϵ and acceptance $\mathcal{A}$, $\mathcal{L}_{95}$ can then be determined by the relationship

$$\mathcal{L}_{95} = \frac{S}{\epsilon \cdot \mathcal{A} \cdot \sigma^{\text{NLO+NNLL}} \times \text{BR} \times \text{BR}}. \quad (96)$$

We then state that a (m_N/M_{W_R}) mass hypothesis is excluded at 95% C.L. if

$$N = \mathcal{L}_{95} \times \sigma^{\text{NLO+NNLL}} \times \text{BR} \times \text{BR} \cdot \epsilon \cdot \mathcal{A} \geq S = 3. \quad (97)$$

For $(m_N/M_{W_R}) \leq 0.1$, we show in Fig. 11(c) that $M_{W_R} < 3(4)[5]$ TeV can be excluded at 95% C.L. with $\mathcal{L} = 0.9(10)[150]$ fb^{-1} of 13 TeV data. Also plotted are the ATLAS experiment's 8 TeV 95% C.L. [54] and KamLAND-Zen 90% C.L. [31,77] complementary exclusion limits. We find that regions of the (M_{W_R}, m_N) parameter space unconstrained by ATLAS and CMS are indeed covered by the present, complementary analysis. The open region between this analysis and ATLAS is an artifact of our choice to limit our study to $(m_N/M_{W_R}) \leq 0.1$; application of the neutrino jet analysis to larger mass ratios will close the region. We note that the ability to exclude $M_{W_R} < 3$ TeV at $\sqrt{s} = 13$ TeV with approximately $1/20$ of the 8 TeV data is consistent with the luminosity increase for DY-type processes [108]. In Fig. 11(d) we show the analogous 100 TeV exclusion potential: with $\mathcal{L} = 100$ fb^{-1} (2.5 ab^{-1}), we find that $M_{W_R} < 22(33)$ TeV and $(m_N/M_{W_R}) \leq 0.1$ can be excluded at 95% C.L.

V. SUMMARY AND CONCLUSION

The origin of tiny, nonzero neutrino masses remains an open question in particle physics. In this study we re-examine the discovery potential of a W_R gauge boson decaying to a heavy Majorana neutrino N in the MLRSM. We focus on the case when N is hierarchically lighter than W_R, i.e., $m_N/M_{W_R} \lesssim 0.1$. In this limit, $W_R \to N$ decays produce highly boosted N that then decay to collimated final states. Subsequently, the canonical collider definition

$$pp \to W_R \to e^{\pm} N (\to e^{\pm} jj) \quad (98)$$

breaks down due to failing isolation criteria of the final-state charged leptons. For such a regime, we consider an alternative collider definition,

$$pp \to W_R \to e^{\pm} N \to e^{\pm} j_N, \quad (99)$$

where j_N is a color-singlet neutrino jet that consists of the collimated N decay products. Furthermore, we consider resummed QCD corrections that are important for high-mass DY processes. We calculate, for the first time, inclusive $pp \to W_R$ production at NLO + NNLL matched to threshold-improved PDFs. This captures dominant contributions beyond NLO, and these are arguably the most precise predictions available for high-mass W_R at 13 and 100 TeV. We summarize our findings:

(1) We introduce the concept of neutrino jets, which has widespread applicability to other processes and models; see Sec. IV A. With our new collider signal definition, a 5–6σ discovery is achievable at 13 TeV with $10(100)[2000]$ fb^{-1} for $M_{W_R} = 3(4)[5]$ TeV and $(m_N/M_{W_R}) < 0.1$. At 100 TeV, a 5σ discovery can be obtained for W_R masses up to $M_{W_R} = 15(30)$ TeV with approximately 100 fb^{-1} (10 ab^{-1}). Conversely, with $0.9(10)[150]$ fb^{-1} of 13 TeV data, $M_{W_R} < 3(4)[5]$ TeV can be excluded at 95% C.L.; with 100 fb^{-1} (2.5 ab^{-1}) of 100 TeV data, $M_{W_R} < 22(33)$ TeV can be excluded. See Sec. IV B.

(2) At 13 TeV the NLO + NNLL contributions increase the Born (NLO)-level predictions by 40–140 (4–70)% for $M_{W_R} = 4 - 5$ TeV, well beyond the NLO scale uncertainty. At 100 TeV threshold effects become important for $M_{W_R} \gtrsim 30$ TeV, where resummation increases the Born (NLO) prediction by $\gtrsim 40(10)\%$. Away from threshold, we find that the resummed result converges to the NLO rate. See Sec. III.

(3) The residual scale dependence at NLO + NNLL for $M_{W_R} = 1$–$5(1$–$30)$ TeV at 13 TeV is maximally subpercent, and $\pm 4\%$ at 100 TeV. The PDF uncertainty at NLO + NNLL exceeds 100% in the threshold regions. Away from threshold, the PDF uncertainty is comparable to the NLO PDF uncertainty. See Sec. III D

ACKNOWLEDGMENTS

We thank B. Pecjak, J. Pavon, J. Rojo, L. Rottoli, C. Tamarit, G. Watt, and C. Wéiland for useful discussions. This work was supported by the UK Science and Technology Facilities Council. M. M. acknowledges support from Royal Society International Exchange Programme and thanks IPPP, Durham University, UK, for hospitality. The work of M. M. is partially supported by the DST INSPIRE Grant No. INSPIRE-15-0074. The work of R. R. is partially supported by the European Union's Horizon 2020 research and innovation program under the Marie Sklodowska-Curie Grant Agreements No. 690575 (InvisiblesPlus RISE) and No. 674896 (Elusives ITN)."

APPENDIX A: THRESHOLD RESUMMATION FOR INCLUSIVE $pp \to W'$ PRODUCTION

Here, we review the details of threshold resummation for inclusive production of W' bosons with arbitrary chiral couplings in pp collisions. Often labeled as soft-gluon or large-x resummation [88–90], the calculation should not be confused with small-k_T (or recoil or Collins-Soper-Sterman) resummation [109–111] nor joint recoil-threshold resummation [112–114]. Many concise texts on the topic exist, e.g., Refs. [91–94,115–117]. We largely follow the notation and spirit of Refs. [91–93] and implement the numerical procedures of Refs. [91,92], but make explicit mass and coupling factors that are often omitted for simplicity.

1. Threshold resummation for W' bosons with arbitrary chiral couplings

The emission of soft gluons from initial-state partons participating in hard, hadronic collisions can spawn large, with respect to the expansion parameter α_s, logarithmic enhancements in scattering cross sections. In certain kinematic configurations, these logarithms can become large enough to render a perturbative expansion unreliable, requiring that the divergent series be summed to all orders. In particular, soft logarithms near the partonic threshold take the form

$$\alpha_s \log\left(\frac{\hat{s}-Q^2}{\hat{s}}\right) = \alpha_s \log(1-z), \qquad z \equiv \frac{Q^2}{\hat{s}}, \tag{A1}$$

where $Q \sim \sqrt{\hat{s}} \gg \Lambda_{\rm QCD}$ is the scale of the hard scattering process, $\sqrt{\hat{s}}$ is the partonic scattering scale, and the dimensionless variable z quantifies the nearness of the partonic scale to the hard scale. A schematic distinction of the hard, partonic, and hadronic scattering (beam) scale $\sqrt{s}$ is illustrated in Fig. 2. The purpose of threshold resummation is to perform a summation of such terms when $z \to 1$ while accounting for the hierarchy of scales via renormalization group evolution (RGE). We now briefly summarize the procedure directly in perturbative QCD (pQCD).

For a generic color-singlet boson $\mathcal{B}$ (scalar or vector) produced in hadron collisions, the total inclusive cross section is given by the usual collinear factorization theorem

$$\sigma^{\rm FO}(h_1 h_2 \to \mathcal{B}+X) = \sum_{a,b=q,\bar{q}',g} \int_{\tau_0}^1 d\tau \mathcal{L}_{ab}(\tau,\mu_f)\hat{\sigma}^{\rm FO}(ab\to\mathcal{B}), \qquad \tau_0 \equiv \frac{M_{\mathcal{B}}^2}{s}, \tag{A2}$$

where the luminosity $\mathcal{L}$ of the parton pair ab, with $a,b \in \{q,\bar{q}',g\}$, at the LHC ($h_1 = h_2 = p$) is given in terms of the PDFs $f_{a/p}$ and $f_{b/p}$ jointly evolved to a factorization scale μ_f:

$$\mathcal{L}_{ab}(\tau,\mu_f) = \frac{1}{1+\delta_{ab}} \int_\tau^1 \frac{d\xi_1}{\xi_1} [f_{a/p}(\xi_1,\mu_f) f_{b/p}(\xi_2,\mu_f) + f_{a/p}(\xi_2,\mu_f) f_{b/p}(\xi_1,\mu_f)], \tag{A3}$$

$$\xi_2 \equiv \frac{\tau}{\xi_1}, \tag{A4}$$

and $\hat{\sigma}^{\rm FO}$ is the FO partonic cross section for the process

$$ab \to \mathcal{B} \quad \text{with} \quad Q = M_{\mathcal{B}}. \tag{A5}$$

Following the notation and methodologies of Refs. [91,93], we account for the arbitrary emission of soft radiation by using a generalization of Eq. (A2):

$$\sigma^{\rm FO}(pp\to\mathcal{B}+X) = \sum_{a,b=q,\bar{q}',g} \int_{\tau_0}^1 d\tau \int_0^1 dz \delta\left(z-\frac{\tau_0}{\tau}\right) \mathcal{L}_{ab}(\tau) \times \hat{\sigma}^{\rm FO}(ab\to\mathcal{B}). \tag{A6}$$

Written this way, we identify the FO partonic cross section in the soft radiation limit as

$$\hat{\sigma}^{\rm FO}(ab\to\mathcal{B}) \equiv \hat{\sigma}^{\rm FO}_{ab} = \sigma_0 \times z \times \Delta^{\rm FO}_{ab}(z), \qquad \Delta^{\rm FO}_{ab}(z) = \sum_{k=0}^{\infty} \left(\frac{\alpha_s}{\pi}\right)^k \Delta^{(k)}_{ab}(z). \tag{A7}$$

The soft threshold coefficient $\Delta_{ab}(z)$, which encapsulates the factorizable soft emissions, is often denoted as C_{ab} and G_{ab} in the literature. For a W' gauge boson with arbitrary chiral couplings g_L and g_R to quarks and mass $M_{\mathcal{B}} = M_{W'}$, the constant term is

$$\sigma_0 = |V^{\rm CKM'}_{ab}|^2 \frac{(g_L^2+g_R^2)\pi}{4N_c M_{W'}^2}. \tag{A8}$$

We suppress the indices on σ_0, as the trivial generalization introduces an unnecessary notational complication. The expression is related to the usual LO partonic expression by

$$\hat{\sigma}^{\rm LO}(q\bar{q}'\to W') = \sigma_0 \times M_{W'}^2 \times \delta(\hat{s}-M_{W'}^2) = \sigma_0 \times z \times \delta(1-z). \tag{A9}$$

At LO, one may identify Δ with the above δ function, which is determined by kinematics alone. This is because the LO $2\to1$ process occurs identically at threshold. Beyond LO the structure of soft logarithms in the perturbative expansion of $\Delta(z)$ remains essentially kinematic in origin [116]. In terms of explicit scale dependence, one can also write Eq. (A7) as

$$\hat{\sigma}^{\rm FO}_{ab} = z \times \Delta^{\rm FO}_{ab}(\hat{s},Q^2) \times \sigma_0(Q^2 = M_{W'}^2). \tag{A10}$$

This suggestive form indeed implies, in the language of RGE, that $\Delta(\hat{s}, Q^2)$ is an evolution operator that runs the hard process at $Q^2 = M_{W'}^2$ up to the partonic scale $\hat{s} = \tau s$ [116].

If working with pQCD, the threshold resummed cross section can be efficiently obtained after writing the hadronic cross section in so-called Mellin (or N or moment) space. This is because such convolutions become products in Mellin space. Applying the Mellin transform, as defined in Eq. (40), to Eq. (A6) with respect to τ_0 yields, for LO W' production,

$$\begin{aligned}\sigma_N^{\mathrm{LO}}(pp \to W') &= \sum_{a,b=q,\bar{q}',g} \int_0^1 d\tau_0 \tau_0^{N-1} \int_{\tau_0}^1 d\tau \\ &\quad \times \int_0^1 dz \delta\left(z - \frac{\tau_0}{\tau}\right) \mathcal{L}_{ab}(\tau) \sigma_0 z \Delta_{ab}^{\mathrm{LO}}(z) \\ &= \sigma_0 \sum_{a,b=q,\bar{q}',g} \mathcal{L}_{ab,(N+1)} \Delta_{ab,(N+1)}^{\mathrm{LO}} \\ &= \sigma_0 \mathcal{L}_{q\bar{q}',(N+1)} \Delta_{q\bar{q}',(N+1)}^{\mathrm{LO}}. \end{aligned} \tag{A11}$$

In the last step we have used the fact that vector boson production is due strictly to $q\bar{q}$ annihilation in the soft limit. This follows from currents of massless fermions being proportional to external fermion energies, i.e., $J^{\mu}_{q_f q_i} \propto \sqrt{E_{q_f} E_{q_i}}$, and therefore, they vanish in the soft radiation limit for initial states $qg, \bar{q}g$ and gg.

Nontrivially, obtaining the resummed cross section in N space is a simple matter of replacing the LO coefficient Δ_N^{LO} in Eq. (A11) by its resummed analogue [88–90]. That is,

$$\sigma_N^{\mathrm{Res.}}(pp \to W') = \sigma_0 \mathcal{L}_{q\bar{q}',(N+1)} \Delta_{q\bar{q}',(N+1)}^{\mathrm{Res.}}. \tag{A12}$$

Among other considerations, the resummation is usually performed in the large-N limit as the $N \to \infty$ limit corresponds to the $z \to 1$ (threshold) limit for partonic cross sections. In this limit, additional gluon emission is constrained to be soft and is therefore exactly where one finds a perturbative expansion rendered unreliable by large logarithms. Specifically, the divergent contributions at leading power in $(1 - z)$ are plus distributions of the form

$$\Delta^{(j)}(z) \sim \alpha_s^j(Q^2) \left[\frac{\log^m(1-z)}{1-z}\right]_+, \quad m \leq 2j - 1. \tag{A13}$$

In Mellin space and in the large-N limit, such distributions are transformed to a series of the form

$$\Delta_N^{(j)} \sim \alpha_s^j(Q^2) \sum_{r=0}^{2j} b_r \log^r N, \tag{A14}$$

where b_r is some N-independent coefficient. To all orders in α_s, resummation captures a number of these divergent logarithms, producing a finite result that can supplement FO calculations. For the kth term in the expansion, resummation corresponds at leading logarithmic accuracy to gathering all logarithms with a power of $r = 2k$; at next-to-leading log accuracy, to all logs such that $2k \geq r \geq 2k - 2$; and generically at N^{j}LL, $2k \geq r \geq 2k - 2j$. Furthermore, this implies that in reexpanding N^{j}LL in α_s, one can identify the inclusive N$^{(j-1)}$LO calculation in the limit where all radiation is soft. This necessitates a matching scheme when combining resummed and FO results beyond LO.

In the notation of Ref. [92], the resummed coefficient $\Delta_N^{\mathrm{Res.}}$ for color-singlet $q\bar{q}'$ pairs is

$$\begin{aligned}\Delta_{q\bar{q}',N}^{\mathrm{Res.}} &= g_0(\alpha_s) \exp \mathcal{S}(\lambda, \bar{\alpha}), \quad \text{with} \\ \lambda &= \bar{\alpha} \log \frac{1}{N} \quad \text{and} \quad \bar{\alpha} = a \alpha_s(Q^2) \beta_0, \end{aligned} \tag{A15}$$

where $a = 2(1)$ for DY (DIS) accounts for the number of contributing initial-state hadrons, and the Sudakov factor $\mathcal{S}$ is given as an expansion in $\bar{\alpha}$, while treating $\bar{\alpha} \ln N \sim \mathcal{O}(1)$:

$$\begin{aligned}\mathcal{S}(\lambda, \bar{\alpha}) &= \sum_{m=0}^{\infty} \bar{\alpha}^{m-1} g_{m+1} \\ &= \underbrace{\underbrace{\underbrace{\frac{1}{\bar{\alpha}} g_1(\lambda)}_{\mathrm{LL}} + g_2(\lambda)}_{\mathrm{NLL}} + \bar{\alpha} g_3(\lambda) + \mathcal{O}(\bar{\alpha}^2)}_{\mathrm{NNLL}} \equiv \sum_{k=0}^{\infty} \alpha_s^k \mathcal{S}_k. \end{aligned} \tag{A16}$$

We note that it is possible to consistently reexpand $\mathcal{S}$ in terms of α_s and coefficients $\mathcal{S}_k$. The normalization function g_0 is similarly perturbative and is given by

$$g_0(\alpha_s) = \sum_{n=0}^{\infty} g_{0n} \alpha_s^n = \underbrace{\underbrace{\underbrace{g_{00}}_{\mathrm{LL}} + \alpha_s g_{01}}_{\mathrm{NLL}} + \alpha_s^2 g_{02}}_{\mathrm{NNLL}} + \mathcal{O}(\alpha_s^3). \tag{A17}$$

Expressions and normalizations for g_m, g_{0n}, and the QCD β-function coefficient β_0 are detailed in [92]. Acquiring a resummation of order[2] N^{j}LL is achieved by including the matching functions in $g_0(\alpha_s)$ up to $\mathcal{O}(\alpha_s^j)$, i.e., all g_{0n} up to $n = j$, and g_m functions for m up to $m = j + 1$. In this work, we resum soft radiation up to NNLL accuracy. Thus our resummed soft function is

[2]In other words, N^{j}LL in the "$*$" convention or N^{j}LL$'$ in the "$'$" convention, which are precisely defined in Ref. [94].

$$\Delta^{\rm NNLL}_{(q\bar{q}')N} = (g_{00} + g_{01}\alpha_s + g_{02}\alpha_s^2) \times \exp\left[\frac{1}{\bar{\alpha}} g_1(\lambda,\bar{\alpha}) + g_2(\lambda,\bar{\alpha}) + \bar{\alpha} g_3(\lambda,\bar{\alpha})\right], \tag{A18}$$

and our resummed cross section in Mellin space at NNLL is

$$\sigma^{\rm NNLL}_N(pp \to W') = \sigma_0 \mathcal{L}_{q\bar{q}',(N+1)} \Delta^{\rm NNLL}_{(q\bar{q}')(N+1)}. \tag{A19}$$

2. Inverse Mellin transformation via minimal prescription procedure

Taking the inverse Mellin transformation of Eq. (A19), as defined in Eq. (41), gives the resummed production cross section in momentum space:

$$\sigma^{\rm Res.}(pp \to W' + X) = \frac{\sigma_0}{2\pi i} \int_{c-i\infty}^{c+i\infty} dN \tau_0^{-(N-1)} \times \mathcal{L}_N \times \Delta_N^{\rm Res.}. \tag{A20}$$

Formally, the integration path, with $c \in \mathbb{R}$, is to the right of all singularities. In practice, this is impossible due to the QCD Landau pole at $N = N_L \equiv \exp[1/2\alpha_s\beta_0]$. The situation can be remedied by adhering to the minimal prescription (MP) procedure [91], which entails choosing $c = C_{\rm MP}$ such that

$$2 < C_{\rm MP} < N_L, \tag{A21}$$

to avoid the Pomeron (Landau) pole as small (large) N, and deforming the path toward $\mathrm{Re}[N] < 0$. The path deformation is illustrated in Fig. 12(b). Subsequently, Eq. (A20) becomes

$$\sigma^{\rm Res.}(pp \to W' + X) \overset{\rm MP}{=} \frac{\sigma_0}{2\pi i} \int_{C_{\rm MP}} dN \tau_0^{-(N-1)} \times \mathcal{L}_N \times \Delta_N^{\rm Res.} \tag{A22}$$

$$= \frac{\sigma_0}{\pi i} \int_{C_{\rm MP}[{\rm Im}[N]>0]} dN \tau_0^{-(N-1)} \times \mathcal{L}_N \times \Delta_N^{\rm Res.}. \tag{A23}$$

In the second line, a factor of 2 follows from the integrand being even with respect to $\mathrm{Im}[N]$. This follows from the fact that the original cross section in momentum space, Eq. (A6), is a real function.

Following Ref. [118], and the associated code `ResHiggs`, we choose the path

$$N(t) = c_{\rm MP} + (m_{\rm MP} - i)\log(t), \qquad t \in (0,1), \tag{A24}$$

where $c_{\rm MP}, m_{\rm MP} \in \mathbb{R}$ cannot be too large numerically without hitting machine precision limitations in $\tau_0^{-(N-1)} = \exp[-(N-1)\log\tau_0]$. We have checked that $5 < c_{\rm MP} < 15$ and $m_{\rm MP} = c_{\rm MP}/10$ leaves the integral unchanged. Making the change of variable to t, one has

$$\sigma^{Res.}(s) = \frac{\sigma_0}{\pi i} \int_0^1 \frac{dt}{t} (i-m) \tau_0^{-(N-1)} \times \mathcal{L}_N \times \Delta_N^{\rm Res.} \tag{A25}$$

$$= \frac{\sigma_0}{\pi} \int_0^1 \frac{dt}{t} {\rm Im}[(i-m) e^{-(N-1)\log\tau_0} \times \mathcal{L}_N \times \Delta_N^{\rm Res.}]. \tag{A26}$$

In the last line, we use the fact that $\sigma^{\rm Res.}$ is a physical rate, i.e., positive definite, implying that the integrand must be purely imaginary to cancel the $1/i$.

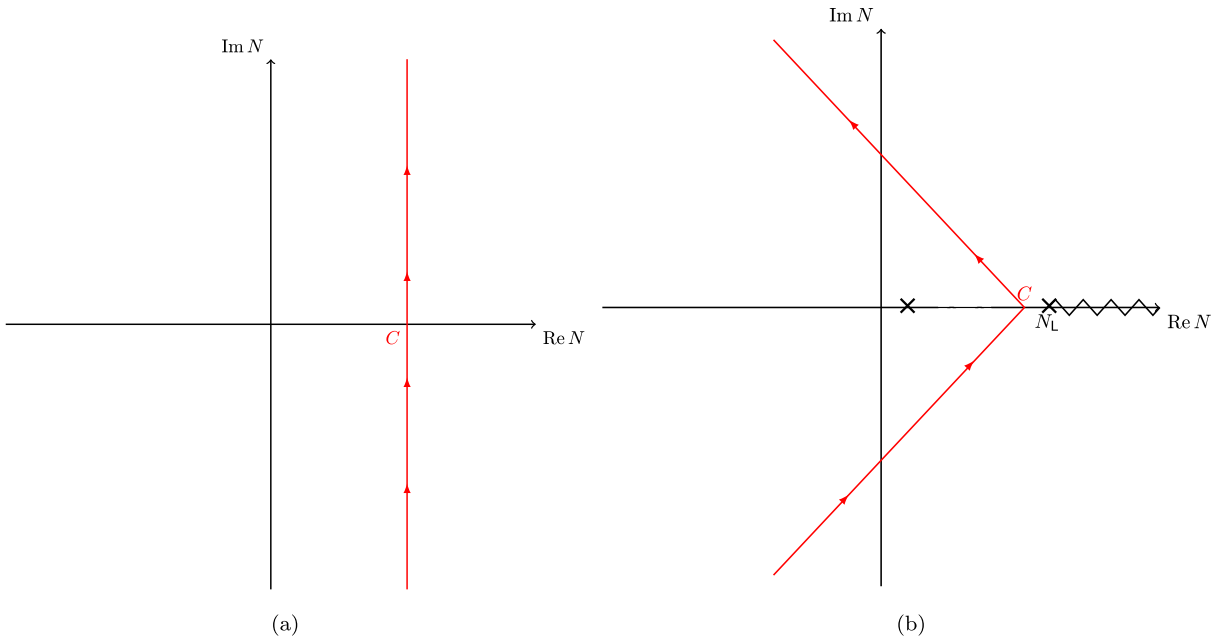

FIG. 12. Contours taken to perform the inverse Mellin transform. In (a) the choice of contour is as defined in Eq. (41). The contour used to implement the minimal prescription for the resummed prediction is shown in (b).

3. Matching resummed and fixed order expressions

The resummation procedure is derived in the threshold limit to leading power in $(1-z)$ and therefore neglects subleading power corrections, e.g., hard, wide-angle radiation. To make viable predictions at collider experiments, it is desirable to supplement resummed formulas with exact FO results beyond LO. This is achievable by subtracting from the resummed expression the $\mathcal{O}(\alpha_s^k)$ radiation terms common to both calculations, to avoid double counting of soft radiation, and add back the full FO $\mathcal{O}(\alpha_s^k)$ result, which describes both soft and hard radiation. A convenient way to isolate those common terms is to Taylor expand the resummed expression $\sigma^{\text{Res.}}$ about $\alpha_s = 0$. Up to NLO, this is given by the first two terms of the expansion

$$\sigma^{\text{Res.}} = \sum_{l=0}^{\infty} \frac{\alpha_s^l}{l!} \left[\frac{\partial^l}{\partial \alpha_s^l} \sigma^{\text{Res.}}\right]_{\alpha_s=0} \tag{A27}$$

$$= \sigma^{\text{Res.}}|_{\alpha_s=0} + \alpha_s [\partial_{\alpha_s} \sigma^{\text{Res.}}]_{\alpha_s=0} + \frac{\alpha_s^2}{2} [\partial^2_{\alpha_s} \sigma^{\text{Res.}}]_{\alpha_s=0} + \mathcal{O}(\alpha_s^3). \tag{A28}$$

As the Mellin and inverse-Mellin operators commute with the ∂_{α_s} operator, the expansion holds in Mellin space. Furthermore, as there is no explicit α_s dependence in σ_0 and $\mathcal{L}_N$ in Eq. (A19), the expansion of $\sigma_N^{\text{Res.}}$ is simply proportional to the Taylor expansion of the exponentiated coefficient $\Delta_N^{\text{Res.}}$. In Mellin space, the $\mathcal{O}(\alpha_s)$-subtracted resummed cross section for $pp \to W_R$ is then

$$\sigma_N^{\text{Res.}}|_{\alpha_s-\text{Subtracted}} = \sigma_0 \times \mathcal{L}_N \times [\Delta_N^{\text{Res.}} - \Delta_N^{\text{Res.}}|_{\alpha_s=0} - \alpha_s [\partial_{\alpha_s} \Delta_N^{\text{Res.}}]_{\alpha_s=0}]. \tag{A29}$$

For color-singlet $q\bar{q}'$ initial states, explicit calculation shows

$$\Delta^{\text{Res.}}_{(q\bar{q}')N}|_{\alpha_s=0} = g_{00} \quad \text{and} \quad \partial_{\alpha_s} \Delta^{\text{Res.}}_{(q\bar{q}')N}|_{\alpha_s=0} = (\mathcal{S}_1 + g_{01}), \tag{A30}$$

which correspond to terms in Eq. (A16) and can be found in [92]. To NLO + NNLL accuracy, the physical inclusive W' production cross section in pp collisions is at last

$$\sigma^{\text{NLO+NNLL}}(pp \to W' + X) = \sigma^{\text{NLO}} + \sigma^{\text{NNLL}}|_{\alpha_s-\text{Subtracted}}, \tag{A31}$$

where the modified resummed term is obtained by inserting Eq. (A29) into Eq. (A26):

$$\sigma^{\text{NNLL}}|_{\alpha_s-\text{Subtracted}} = \frac{\sigma_0}{\pi} \int_0^1 \frac{dt}{t} \text{Im}[(i-m)\tau_0^{-(N-1)} \times \mathcal{L}_N \times (\Delta^{\text{NNLL}}_{(q\bar{q}')N} - g_{00} - \alpha_s(\mathcal{S}_1 + g_{01}))]. \tag{A32}$$

4. Parton luminosities in Mellin space

The resummation formalism we exploit requires parton luminosities $\mathcal{L}_{q\bar{q}'}$ in Mellin space. This introduces a technical difficulty as modern PDF sets are typically only available numerically. It is possible, however, at a fixed factorization scale μ_f, to approximate luminosities $\mathcal{L}_{ab}(\tau)$ [and individual PDFs $f_{a/p}(\xi)$] using a basis of polynomials that can be Mellin transformed analytically. Here we use a basis of Chebyshev polynomials of the first kind $T_n(x)$, for which fast numerical algorithms exist for calculating the expansion coefficients, e.g. [119]. The implementation and optimization of the Chebyshev approximation procedure has been documented in Refs. [92,94]. We briefly summarize, for completeness, how to obtain the approximated $\mathcal{L}_{(q\bar{q}')N}$.

We write a general Chebyshev polynomial of degree n defined over the domain $x \in (-1, 1)$ as

$$T_n(x) = \sum_{m=0}^{n} T_{mn} x^n, \qquad T_{mn} \in \mathbb{Z}.$$

The function $F(u)$ over the domain $u \in (u_{\min}, u_{\max})$ can then be approximated by the first n_{ch} polynomials by the relationship

$$F(u) \approx -\frac{c_0}{2} + \sum_{k=0}^{n_{ch}} c_k T_k(Au + B), \tag{A33}$$

with A and B given by

$$A = \frac{2}{u_{\max} - u_{\min}} \quad \text{and} \quad B = -\frac{u_{\max} + u_{\min}}{u_{\max} - u_{\min}}, \tag{A34}$$

and the kth Chebyshev coefficient c_k by [119]

$$c_k = \frac{2}{n_{ch}+1} \sum_{j=0}^{n_{ch}} \tilde{F}_j \times \cos\left(\frac{k\pi(j+\frac{1}{2})}{n_{ch}+1}\right). \tag{A35}$$

The jth moment of $F(u)$, i.e., $\tilde{F}_j$, is defined as

$$\tilde{F}_j = F(y_j), \quad \text{with} \quad y_j = \frac{1}{2}(u_{\max} - u_{\min}) \cos\left(\frac{\pi(j+\frac{1}{2})}{n_{ch}+1}\right) + \frac{(u_{\max} + u_{\min})}{2}. \tag{A36}$$

Such efficient algorithms allow us, in principle, to immediately obtain the luminosity $\mathcal{L}_{q\bar{q}'}(\tau, \mu_f)$ in Mellin space by transforming Eq. (A33) directly. However, $\mathcal{L}(\tau)$ is generally poorly behaved across $\tau \in (0, 1)$, particularly at the origin. This is resolvable by approximating a regularized version of the luminosity and setting

$$F(u) = \tau(u)\mathcal{L}_{q\bar{q}'}(\tau(u), \mu_f), \quad \text{with}$$
$$\tau(u) = e^u \quad \text{for } u \in (\log\tau_0, 0). \tag{A37}$$

As defined in Eq. (30), $\tau_0 = M_{W'}^2/s$ is the threshold above which $pp \to W'$ is kinematically allowed to proceed. After a wee bit of algebra, we obtain an expression for the Mellin-transformed parton luminosities,

$$\begin{aligned}\mathcal{L}_{(q\bar{q}')N} &= \int_0^1 d\tau \tau^{N-1}\mathcal{L}_{q\bar{q}'}(\tau, \mu_f) \\ &= \int_0^1 d\tau(u)\tau^{N-2}(u)F(u) \\ &= \sum_{p=0}^{n_{ch}} \frac{\bar{c}_p}{(N-1)^{p+1}},\end{aligned} \tag{A38}$$

where we have defined

$$\bar{c}_p = \frac{2^p}{u_{\min}^p}\sum_{j=p}^{n_{ch}} \frac{j!}{(j-p)!}\tilde{c}_j, \quad \text{with}$$
$$\tilde{c}_j = -\frac{c_0}{2}\delta_{j0} + \sum_{k=j}^{n_{ch}} c_k T_{kj}. \tag{A39}$$

Once one calculates the initial coefficients c_i, it is straightforward to approximate the Mellin transform of $\mathcal{L}_{q\bar{q}'}(\tau, \mu_f)$ by using Eqs. (A38) and (A39). However, for different μ_f choices, the function being approximated changes, and therefore the coefficients c_k need to be recomputed. This should be taken into account if one intends to use a dynamic factorization scale.

APPENDIX B: MODELING MANIFEST LEFT-RIGHT SYMMETRIC MODEL WITH FEYNRULES

The most generic scalar potential of the LRSM consists of 18 parameters: three mass scales $\mu_{1,\ldots,3}$, 14 dimensionless couplings $\lambda_{1,\ldots,4}$, $\rho_{1,\ldots,4}$, $\alpha_{1,\ldots,3}$, $\beta_{1,\ldots,3}$, and one CP violating phase δ_2. It is given by [120]

$$V(\Phi, \Delta_L, \Delta_R) = V_\mu + V_\Phi + V_\Delta + V_{\Phi\Delta} + V_{\Phi\Delta_L\Delta_R}, \tag{B1}$$

where the scalar mass and self-coupling terms of the bidoublet Φ are, respectively,

$$\begin{aligned}V_\mu = &-\mu_1^2\mathrm{Tr}[\Phi^\dagger\Phi] - \mu_2^2\mathrm{Tr}[\Phi^\dagger\tilde{\Phi} + \tilde{\Phi}^\dagger\Phi] \\ &- \mu_3^2\mathrm{Tr}[\Delta_L^\dagger\Delta_L + \Delta_R^\dagger\Delta_R],\end{aligned} \tag{B2}$$

$$\begin{aligned}V_\Phi = &\lambda_1[\mathrm{Tr}[\Phi^\dagger\Phi]]^2 + \lambda_2[\mathrm{Tr}[\Phi^\dagger\tilde{\Phi}]]^2 + \lambda_2[\mathrm{Tr}[\tilde{\Phi}^\dagger\Phi]]^2 \\ &+ \lambda_3\mathrm{Tr}[\Phi^\dagger\tilde{\Phi}]\mathrm{Tr}[\tilde{\Phi}^\dagger\Phi] + \lambda_4\mathrm{Tr}[\Phi^\dagger\Phi]\mathrm{Tr}[\Phi^\dagger\tilde{\Phi} + \tilde{\Phi}^\dagger\Phi].\end{aligned} \tag{B3}$$

The $\Delta_{L,R}$ self- and cross-couplings are

$$\begin{aligned}V_\Delta = &\rho_1[\mathrm{Tr}[\Delta_L^\dagger\Delta_L]]^2 + \rho_1[\mathrm{Tr}[\Delta_R^\dagger\Delta_R]]^2 \\ &+ \rho_3\mathrm{Tr}[\Delta_L^\dagger\Delta_L]\mathrm{Tr}[\Delta_R^\dagger\Delta_R] \\ &+ \rho_2\mathrm{Tr}[\Delta_L\Delta_L]\mathrm{Tr}[\Delta_L^\dagger\Delta_L^\dagger] + \rho_2\mathrm{Tr}[\Delta_R\Delta_R]\mathrm{Tr}[\Delta_R^\dagger\Delta_R^\dagger] \\ &+ \rho_4\mathrm{Tr}[\Delta_L\Delta_L]\mathrm{Tr}[\Delta_R^\dagger\Delta_R^\dagger] + \rho_4\mathrm{Tr}[\Delta_L^\dagger\Delta_L^\dagger]\mathrm{Tr}[\Delta_R\Delta_R].\end{aligned} \tag{B4}$$

The $\Phi - \Delta_L$ and $\Phi - \Delta_R$ couplings are

$$\begin{aligned}V_{\Phi\Delta} = &\alpha_1\mathrm{Tr}[\Phi^\dagger\Phi]\mathrm{Tr}[\Delta_L^\dagger\Delta_L + \Delta_R^\dagger\Delta_R] \\ &+ \alpha_3\mathrm{Tr}[\Phi\Phi^\dagger\Delta_L\Delta_L^\dagger + \phi^\dagger\phi\Delta_R\Delta_R^\dagger] \\ &+ \{\alpha_2 e^{i\delta_2}\mathrm{Tr}[\Phi^\dagger\tilde{\Phi}]\mathrm{Tr}[\Delta_L^\dagger\Delta_L] \\ &+ \alpha_2 e^{i\delta_2}\mathrm{Tr}[\tilde{\Phi}^\dagger\Phi]\mathrm{Tr}[\Delta_R^\dagger\Delta_R] + \text{H.c.}\},\end{aligned} \tag{B5}$$

with $\delta_2 = 0$ making CP conservation explicit, and the $\Phi - \Delta_L - \Delta_R$ couplings are

$$\begin{aligned}V_{\Phi\Delta_L\Delta_R} = &\beta_1\mathrm{Tr}[\Phi^\dagger\Delta_L^\dagger\Phi\Delta_R + \Delta_R^\dagger\Phi^\dagger\Delta_L\Phi] \\ &+ \beta_2\mathrm{Tr}[\Phi^\dagger\Delta_L^\dagger\tilde{\Phi}\Delta_R + \Delta_R^\dagger\tilde{\Phi}^\dagger\Delta_L\Phi] \\ &+ \beta_3\mathrm{Tr}[\tilde{\Phi}^\dagger\Delta_L^\dagger\Phi\Delta_R + \Delta_R^\dagger\Phi^\dagger\Delta_L\tilde{\Phi}].\end{aligned} \tag{B6}$$

After LR and EWSB, there exists 10 physical scalars: four neutral, CP even states $H^0_{0,\ldots,3}$, including one at $m_{H_0^0} \approx 125$ GeV; two neutral CP odd states $A^0_{0,1}$; two states singly charged under $U(1)_{\mathrm{EM}}$ $H^\pm_{1,2}$; and two doubly charged states $\delta^{\pm\pm}_{L,R}$. Subscripts do not indicate a mass ordering. The mass spectrum in the VEV limit of Eq. (12) is given by [21,120]

$$\begin{aligned}&m^2_{H_0^0} \approx (125\ \text{GeV})^2 \approx 2k_+^2\left(\lambda_1 + 4\frac{k_1^2k_2^2}{k_+^4}(2\lambda_2 + \lambda_3) + 4\lambda_4\frac{k_1k_2}{k_+^2}\right), \\ &M^2_{H_1^0} = M^2_{A_1^0} \approx \alpha_3\frac{v_R^2}{2}\frac{k_+^2}{k_-^2}, \qquad M^2_{H_3^0} = M^2_{A_2^0} \approx (\rho_3 - 2\rho_1)\frac{v_R^2}{2}, \qquad M^2_{H_2^0} \approx 2\rho_1 v_R^2, \\ &M^2_{H_1^\pm} \approx (\rho_3 - 2\rho_1)\frac{v_R^2}{2} + \alpha_3\frac{k_-^2}{4}, \qquad M^2_{\delta_L^{\pm\pm}} \approx (\rho_3 - 2\rho_1)\frac{v_R^2}{2} + \alpha_3\frac{k_-^2}{2}, \\ &M^2_{H_2^\pm} \approx \alpha_3\frac{v_R^2}{2}\frac{k_+^2}{k_-^2} + \alpha_3\frac{k_-^2}{4}, \qquad M^2_{\delta_R^{\pm\pm}} \approx 2\rho_2 v_R^2 + \alpha_3\frac{k_-^2}{2},\end{aligned} \tag{B7}$$

where $k_\pm$ is defined in Eq. (7).

With choice assumptions, the potential can be configured such that the theory is consistent with experimental limits and features new gauge states accessible by the LHC or VLHC. Accordingly, the Manifest LRSM FeynRules model of [73] can be set to simulate this region of the MLRSM parameter space. We now discuss this configuration.

1. Phenomenological constraints on LRSM scalar potential

Explicit CP conservation and minimization conditions of the potential give rise to the so-called VEV seesaw relationship [120]:

$$v_L = \frac{\beta_2 k_1^2 + \beta_1 k_1 k_2 + \beta_3 k_2^2}{(2\rho_1 - \rho_3) v_R}, \tag{B8}$$

implying inherently small v_L for $2\rho_1 \neq \rho_3$ and $v_R^2 \gg k_1, k_2$. Though it is natural for all ρ_i to be comparable in magnitude, it is contrived to expect a fine cancellation, particularly after radiative corrections. Consistent with ρ/T-parameter measurements [22,25], we choose

$$v_L = 0 \Leftrightarrow \beta_{1,\ldots,3} = 0. \tag{B9}$$

This may also be achievable if Eq. (B1) respects an approximate custodial symmetry.

Neglecting terms $\mathcal{O}(k_+^2/v_R^2)$, the minimization conditions also imply [120]

$$\begin{aligned} \frac{\mu_1^2}{v_R^2} &= \frac{\alpha_1}{2} - \frac{\alpha_3}{2}\left(\frac{k_2^2}{k_-^2}\right), \\ \frac{\mu_2^2}{v_R^2} &= \frac{\alpha_1}{2} + \frac{\alpha_3}{4}\left(\frac{k_1 k_2}{k_-^2}\right), \\ \frac{\mu_3^2}{v_R^2} &= \rho_1. \end{aligned} \tag{B10}$$

As argued, one expects, on naturalness grounds,

$$\alpha_{2,3} \sim \mathcal{O}(\alpha_1) \quad \text{and} \quad \rho_{2,3} \sim \mathcal{O}(\rho_1). \tag{B11}$$

Dropping terms relatively suppressed by $(k_2/k_-) \sim (m_b/m_t) \sim 10^{-2}$ [see Eq. (8)] gives

$$\frac{\mu_1^2}{v_R^2} \approx \frac{\mu_2^2}{v_R^2} \approx \frac{\alpha_1}{2}, \qquad \frac{\mu_3^2}{v_R^2} = \rho_1, \tag{B12}$$

suggesting that LRSB is inherently at the mass scale of the scalar potential assuming

$$\alpha_1 \sim \mathcal{O}(1) \quad \text{and} \quad \rho_1 \sim \mathcal{O}(1). \tag{B13}$$

In terms of M_{W_R} and g, Eq. (B13) and positivity of squared masses for (physical) scalars imply several mass and coupling relationships:

$$\begin{aligned} &\frac{m_{H_1^0}^2}{M_{W_R}^2}, \frac{m_{A_1^0}^2}{M_{W_R}^2}, \frac{m_{H_2^\pm}^2}{M_{W_R}^2} \approx \frac{\alpha_3}{g^2} > 1, \\ &\frac{m_{H_2^0}^2}{M_{W_R}^2} \approx \frac{4\rho_1}{g^2} > 1, \\ &\frac{m_{H_3^0}^2}{M_{W_R}^2}, \frac{m_{A_2^0}^2}{M_{W_R}^2}, \frac{m_{H_1^\pm}^2}{M_{W_R}^2}, \frac{m_{\delta_L^{\pm\pm}}^2}{M_{W_R}^2} \approx \frac{(\rho_3 - 2\rho_1)}{g^2} > 0, \\ &\frac{m_{\delta_R^{\pm\pm}}^2}{M_{W_R}^2} \approx \frac{4\rho_2}{g^2} > 1. \end{aligned} \tag{B14}$$

Imposing the strong requirement on Eq. (B14) to universally comply with bounds on FCNH, i.e., m_{FCNH} in Eq. (24), implies

$$\rho_{1,2,4} > \frac{g^2}{4}\left(\frac{m_{\text{FCNH}}}{M_{W_R}}\right)^2, \quad \rho_3 > g^2\left(\frac{m_{\text{FCNH}}}{M_{W_R}}\right)^2 + 2\rho_1 \sim 6\rho_1, \tag{B15}$$

$$\alpha_{1,\ldots,3} > g^2\left(\frac{m_{\text{FCNH}}}{M_{W_R}}\right)^2, \qquad \mu_{1,2}^2 > (m_{\text{FCNH}})^2, \qquad \mu_3^2 > \frac{1}{2}(m_{\text{FCNH}})^2. \tag{B16}$$

Several observations can be made from these relations: First is that for $M_{W_R} \lesssim 6.5$ TeV, one has $\rho_{1,2,4} > 1$. Thus, discovery of a W_R at the LHC would indicate a strongly coupled triplet sector. Second is that a small hierarchy among the ρ_i may exist. Requiring both H_2^0 and H_3^0 to be heavier than m_{FCNH} suggests $\rho_3 \gtrsim 6\rho_1$. Figure 13 plots the values of ρ_3 for given M_{W_R} and m_{FCNH}, and shows, for example, that $\rho_3 < 1$ and $m_{\text{FCNH}} \sim 15(20)$ TeV require

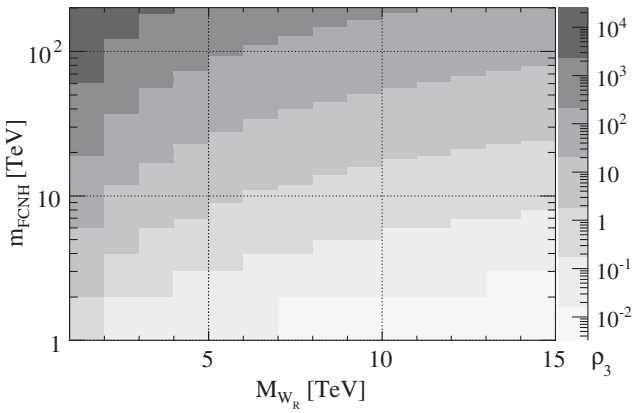

FIG. 13. Scalar triplet coupling ρ_3 contours for given M_{W_R} and m_{FCNH}.

$M_{W_R} \gtrsim 10(12)$ TeV. If H_3^0 and A_2^0 are largely responsible for neutral flavor transitions, then $\rho_{1,3}$ can be reduced while keeping their differences fixed. We do not apply theoretical prejudices against strongly coupled systems, and we treat this as a consistent prediction. A more detailed discussion on the perturbativity of the scalar sector can be found in [52].

An ambiguity arises for the bidoublet self-couplings $\lambda_{1,3,4}$ as the self-coupling of the SM-like Higgs is unconstrained. Using Eq. (B7), we take, without impacting our study,

$$\lambda_1 \approx \frac{m_{H_0^0}^2}{2k_+^2}, \qquad \lambda_{2,3} = 0. \tag{B17}$$

2. Configuration of LRSM FeynRules file

We implement our configuration of the scalar potential and choice for quark and lepton mixing into one FR restriction file that can be invoked when generating UFOs for the Manifest LRSM v1.1.6-MIX model file by [73]. See [96] for instructions. Internal parameters, e.g., v_R and SM inputs of Eq. (28), can be modified via MG5 input parameter cards. The restriction file, `lrsmLHCRestrictions.rst`, is available from the source directory for the arXiv preprint version of this report. It contains the following parameter identifications:

```
  (* Turn off CKM mixing *)
  s12 -> 0,
  s23 -> 0,
  s13 -> 0,
  (* Turn off light neutrino mixing and set
PMNS to diagonal *)
  sL13 -> 0,
  sL23 -> 0,
  sL13 -> 0,
  (* Turn off off-diagonal heavy/light neu-
trino mixing [V,X in Eq.(A.11) of
0901.3589] *)
  VKe -> 0,
  VKmu -> 0,
  VKta -> 0,
  (* Make mixing in LRSM manifest: all +1.
Quasi-manifest: at least one -1 *)
  Wl11 -> 1,
  Wl22 -> 1,
  Wl33 -> 1,
  WU11 -> 1,
  WU22 -> 1,
  WU33 -> 1,
  WD11 -> 1,
  WD22 -> 1,
  WD33 -> 1,
  (* LH vev *)
  vL -> 0,
  (* Quark masses and Yukawas *)
  MU -> 0,
  MD -> 0,
  MC -> 0,
  MS -> 0,
  (* Lepton masses and Yukawas *)
  Me -> 0,
  Mmu -> 0,
  Mta -> 0,
  MN1 -> 0,
  MN2 -> 0,
  MN3 -> 0.
```


[1] S. Weinberg, Baryon and Lepton Nonconserving Processes, Phys. Rev. Lett. **43**, 1566 (1979).

[2] F. Wilczek and A. Zee, Operator Analysis of Nucleon Decay, Phys. Rev. Lett. **43**, 1571 (1979).

[3] E. Ma, Pathways to Naturally Small Neutrino Masses, Phys. Rev. Lett. **81**, 1171 (1998).

[4] P. Minkowski, $\mu \to e\gamma$ at a rate of one out of 10^9 muon decays?, Phys. Lett. **67B**, 421 (1977).

[5] R. N. Mohapatra and G. Senjanovic, Neutrino Mass and Spontaneous Parity Violation, Phys. Rev. Lett. **44**, 912 (1980).

[6] T. Yanagida, Horizontal symmetry and masses of neutrinos, Conference Proceedings **C7902131**, 95 (1979).

[7] M. Gell-Mann, P. Ramond, and R. Slansky, Complex spinors and unified theories, Conference Proceedings **C790927**, 315 (1979).

[8] J. Schechter and J. W. F. Valle, Neutrino masses in $SU(2) \times U(1)$ theories, Phys. Rev. D **22**, 2227 (1980).

[9] R. E. Shrock, General theory of weak leptonic and semileptonic decays. 1. Leptonic pseudoscalar meson decays, with associated tests for, and bounds on, neutrino masses and lepton mixing, Phys. Rev. D **24**, 1232 (1981).

[10] M. Magg and C. Wetterich, Neutrino mass problem and gauge hierarchy, Phys. Lett. **94B**, 61 (1980).

[11] T. P. Cheng and L. F. Li, Neutrino masses, mixings, and oscillations in $SU(2) \times U(1)$ models of electroweak interactions, Phys. Rev. D **22**, 2860 (1980).

[12] G. Lazarides, Q. Shafi, and C. Wetterich, Proton lifetime and fermion masses in an SO(10) model, Nucl. Phys. **B181**, 287 (1981).

[13] R. N. Mohapatra and G. Senjanovic, Neutrino masses and mixings in gauge models with spontaneous parity violation, Phys. Rev. D **23**, 165 (1981).
[14] R. Foot, H. Lew, X. G. He, and G. C. Joshi, Seesaw neutrino masses induced by a triplet of leptons, Z. Phys. C **44**, 441 (1989).
[15] N. Arkani-Hamed, T. Han, M. Mangano, and L. T. Wang, Physics opportunities of a 100 TeV proton-proton collider, Phys. Rep. **652**, 1 (2016).
[16] T. Golling *et al.*, Physics at a 100 TeV pp collider: Beyond the Standard Model phenomena, arXiv:1606.00947.
[17] M. C. Chen and J. Huang, TeV scale models of neutrino masses and their phenomenology, Mod. Phys. Lett. A **26**, 1147 (2011).
[18] J. C. Pati and A. Salam, Lepton number as the fourth color, Phys. Rev. D **10**, 275 (1974); **11**, 703(E) (1975).
[19] R. N. Mohapatra and J. C. Pati, A natural left-right symmetry, Phys. Rev. D **11**, 2558 (1975).
[20] G. Senjanovic and R. N. Mohapatra, Exact left-right symmetry and spontaneous violation of parity, Phys. Rev. D **12**, 1502 (1975).
[21] P. Duka, J. Gluza, and M. Zralek, Quantization and renormalization of the manifest left-right symmetric model of electroweak interactions, Ann. Phys. (N.Y.) **280**, 336 (2000).
[22] M. C. Chen, S. Dawson, and T. Krupovnickas, Constraining new models with precision electroweak data, Int. J. Mod. Phys. A **21**, 4045 (2006).
[23] Y. Zhang, H. An, X. Ji, and R. N. Mohapatra, Right-handed quark mixings in minimal left-right symmetric model with general CP violation, Phys. Rev. D **76**, 091301 (2007).
[24] Y. Zhang, H. An, X. Ji, and R. N. Mohapatra, General *CP* violation in minimal left-right symmetric model and constraints on the right-handed scale, Nucl. Phys. **B802**, 247 (2008).
[25] M. C. Chen, S. Dawson, and C. B. Jackson, Higgs triplets, decoupling, and precision measurements, Phys. Rev. D **78**, 093001 (2008).
[26] V. Tello, M. Nemevsek, F. Nesti, G. Senjanovic, and F. Vissani, Left-Right Symmetry: From LHC to Neutrinoless Double Beta Decay, Phys. Rev. Lett. **106**, 151801 (2011).
[27] M. Nemevsek, F. Nesti, G. Senjanovic, and V. Tello, Neutrinoless double beta decay: Low left-right symmetry scale?, arXiv:1112.3061.
[28] F. F. Deppisch, M. Hirsch, and H. Pas, Neutrinoless double beta decay and physics beyond the standard model, J. Phys. G **39**, 124007 (2012).
[29] J. Chakrabortty, H. Z. Devi, S. Goswami, and S. Patra, Neutrinoless double-β decay in TeV scale left-right symmetric models, J. High Energy Phys. 08 (2012) 008.
[30] M. Nemevsek, G. Senjanovic, and V. Tello, Connecting Dirac and Majorana Neutrino Mass Matrices in the Minimal Left-Right Symmetric Model, Phys. Rev. Lett. **110**, 151802 (2013).
[31] P. S. Bhupal Dev, S. Goswami, M. Mitra, and W. Rodejohann, Constraining neutrino mass from neutrinoless double beta decay, Phys. Rev. D **88**, 091301 (2013).
[32] R. L. Awasthi, A. Dasgupta, and M. Mitra, Limiting the effective mass and new physics parameters from $0\nu\beta\beta$, Phys. Rev. D **94**, 073003 (2016).
[33] J. Barry and W. Rodejohann, Lepton number and flavour violation in TeV-scale left-right symmetric theories with large left-right mixing, J. High Energy Phys. 09 (2013) 153.
[34] A. Maiezza and M. Nemevsek, Strong P invariance, neutron electric dipole moment, and minimal left-right parity at LHC, Phys. Rev. D **90**, 095002 (2014).
[35] S. Bertolini, A. Maiezza, and F. Nesti, Present and future K and B meson mixing constraints on TeV scale left-right symmetry, Phys. Rev. D **89**, 095028 (2014).
[36] R. L. Awasthi, P. S. B. Dev, and M. Mitra, Implications of the diboson excess for neutrinoless double beta decay and lepton flavor violation in TeV scale left-right symmetric model, Phys. Rev. D **93**, 011701 (2016).
[37] W. Y. Keung and G. Senjanovic, Majorana Neutrinos and the Production of the Right-Handed Charged Gauge Boson, Phys. Rev. Lett. **50**, 1427 (1983).
[38] A. Ferrari, J. Collot, M. L. Andrieux, B. Belhorma, P. de Saintignon, J. Y. Hostachy, P. Martin, and M. Wielers, Sensitivity study for new gauge bosons and right-handed Majorana neutrinos in pp collisions at $s = 14$-TeV, Phys. Rev. D **62**, 013001 (2000).
[39] M. Frank, A. Hayreter, and I. Turan, Production and decays of W_R bosons at the LHC, Phys. Rev. D **83**, 035001 (2011).
[40] S. P. Das, F. F. Deppisch, O. Kittel, and J. W. F. Valle, Heavy neutrinos and lepton flavour violation in left-right symmetric models at the LHC, Phys. Rev. D **86**, 055006 (2012).
[41] T. Han, I. Lewis, R. Ruiz, and Z. g. Si, Lepton number violation and W' chiral couplings at the LHC, Phys. Rev. D **87**, 035011 (2013).
[42] C. Y. Chen, P. S. B. Dev, and R. N. Mohapatra, Probing heavy-light neutrino mixing in left-right seesaw models at the LHC, Phys. Rev. D **88**, 033014 (2013).
[43] P. S. Bhupal Dev, C. H. Lee, and R. N. Mohapatra, Leptogenesis constraints on the mass of right-handed gauge bosons, Phys. Rev. D **90**, 095012 (2014).
[44] J. C. Vasquez, Right-handed lepton mixings at the LHC, J. High Energy Phys. 05 (2016) 176.
[45] A. Maiezza, M. Nemevsek, and F. Nesti, Lepton Number Violation in Higgs Decay at LHC, Phys. Rev. Lett. **115**, 081802 (2015).
[46] J. Gluza and T. Jeliński, Heavy neutrinos and the pp → lljj CMS data, Phys. Lett. B **748**, 125 (2015).
[47] J. Chakrabortty, J. Gluza, T. Jeliński, and T. Srivastava, Theoretical constraints on masses of heavy particles in left-right symmetric models, Phys. Lett. B **759**, 361 (2016).
[48] P. S. B. Dev, D. Kim, and R. N. Mohapatra, Disambiguating seesaw models using invariant mass variables at hadron colliders, J. High Energy Phys. 01 (2016) 118.
[49] J. N. Ng, A. de la Puente, and B. W. P. Pan, Search for heavy right-handed neutrinos at the LHC and beyond in the same-sign same-flavor leptons final state, J. High Energy Phys. 12 (2015) 172.

[50] S. Mondal and S. K. Rai, Polarized window for left-right symmetry and a right-handed neutrino at the Large Hadron-Electron Collider, Phys. Rev. D **93**, 011702 (2016).
[51] M. Lindner, F. S. Queiroz, W. Rodejohann, and C. E. Yaguna, Left-right symmetry and lepton number violation at the Large Hadron Electron Collider, J. High Energy Phys. 06 (2016) 140.
[52] A. Maiezza, M. Nemevsek, and F. Nesti, Perturbativity and mass scales of left-right Higgs bosons, Phys. Rev. D **94**, 035008 (2016).
[53] P. Fileviez Perez, C. Murgui, and S. Ohmer, Simple left-right theory: Lepton number violation at the LHC, Phys. Rev. D **94**, 051701 (2016).
[54] G. Aad *et al.* (ATLAS Collaboration), Search for heavy Majorana neutrinos with the ATLAS detector in pp collisions at $\sqrt{s} = 8$ TeV, J. High Energy Phys. 07 (2015) 162.
[55] V. Khachatryan *et al.* (CMS Collaboration), Search for heavy neutrinos and W bosons with right-handed couplings in proton-proton collisions at $\sqrt{s} = 8$ TeV, Eur. Phys. J. C **74**, 3149 (2014).
[56] S. Patra, F. S. Queiroz, and W. Rodejohann, Stringent dilepton bounds on left-right models using LHC data, Phys. Lett. B **752**, 186 (2016).
[57] M. Lindner, F. S. Queiroz, and W. Rodejohann, Dilepton bounds on left-right symmetry at the LHC run II and neutrinoless double beta decay, Phys. Lett. B **762**, 190 (2016).
[58] G. Aad *et al.* (ATLAS Collaboration), Search for new phenomena in dijet mass and angular distributions from pp collisions at $\sqrt{s} = 13$ TeV with the ATLAS detector, Phys. Lett. B **754**, 302 (2016).
[59] V. Khachatryan *et al.* (CMS Collaboration), Search for Narrow Resonances Decaying to Dijets in Proton-Proton Collisions at $\sqrt{(s)} = 13$ TeV, Phys. Rev. Lett. **116**, 071801 (2016).
[60] T. Jezo, M. Klasen, D. R. Lamprea, F. Lyonnet, and I. Schienbein, NLO + NLL limits on W' and Z' gauge boson masses in general extensions of the Standard Model, J. High Energy Phys. 12 (2014) 092.
[61] D. Binosi and L. Theussl, JaxoDraw: A graphical user interface for drawing Feynman diagrams, Comput. Phys. Commun. **161**, 76 (2004).
[62] CMS Collaboration, Report No. CMS-PAS-EXO-15-006.
[63] Z. Kang, P. Ko, and J. Li, New avenues to heavy right-handed neutrinos with pair production at hadronic colliders, Phys. Rev. D **93**, 075037 (2016).
[64] D. E. Kaplan, K. Rehermann, M. D. Schwartz, and B. Tweedie, Top Tagging: A Method for Identifying Boosted Hadronically Decaying Top Quarks, Phys. Rev. Lett. **101**, 142001 (2008).
[65] T. Plehn, G. P. Salam, and M. Spannowsky, Fat Jets for a Light Higgs, Phys. Rev. Lett. **104**, 111801 (2010).
[66] T. Plehn, M. Spannowsky, M. Takeuchi, and D. Zerwas, Stop reconstruction with tagged tops, J. High Energy Phys. 10 (2010) 078.
[67] D. E. Soper and M. Spannowsky, Finding top quarks with shower deconstruction, Phys. Rev. D **87**, 054012 (2013).
[68] S. Schaetzel and M. Spannowsky, Tagging highly boosted top quarks, Phys. Rev. D **89**, 014007 (2014).
[69] M. Bonvini, S. Marzani, J. Rojo, L. Rottoli, M. Ubiali, R. D. Ball, V. Bertone, S. Carrazza, and N. P. Hartland, Parton distributions with threshold resummation, J. High Energy Phys. 09 (2015) 191.
[70] W. Beenakker, C. Borschensky, M. Krämer, A. Kulesza, E. Laenen, S. Marzani, and J. Rojo, NLO + NLL squark and gluino production cross-sections with threshold-improved parton distributions, Eur. Phys. J. C **76**, 53 (2016).
[71] Z. Sullivan, Fully differential W' production and decay at next-to-leading order in QCD, Phys. Rev. D **66**, 075011 (2002).
[72] S. Quackenbush, R. Gavin, Y. Li, and F. Petriello, W physics at the LHC with FEWZ 2.1, Comput. Phys. Commun. **184**, 209 (2013).
[73] A. Roitgrund, G. Eilam, and S. Bar-Shalom, Implementation of the left-right symmetric model in FeynRules/CalcHep, arXiv:1401.3345.
[74] J. G. Korner, A. Pilaftsis, and K. Schilcher, Leptonic CP asymmetries in flavor changing H^0 decays, Phys. Rev. D **47**, 1080 (1993).
[75] W. Grimus and L. Lavoura, The seesaw mechanism at arbitrary order: Disentangling the small scale from the large scale, J. High Energy Phys. 11 (2000) 042.
[76] A. Atre, T. Han, S. Pascoli, and B. Zhang, The search for heavy Majorana neutrinos, J. High Energy Phys. 05 (2009) 030.
[77] A. Gando *et al.* (KamLAND-Zen Collaboration), Search for Majorana Neutrinos Near the Inverted Mass Hierarchy Region with KamLAND-Zen, Phys. Rev. Lett. **117**, 082503 (2016).
[78] K. A. Olive *et al.* (Particle Data Group Collaboration), Review of particle physics, Chin. Phys. C **38**, 090001 (2014).
[79] A. Buckley, J. Ferrando, S. Lloyd, K. Nordström, B. Page, M. Rfenacht, M. Schnherr, and G. Watt, LHAPDF6: Parton density access in the LHC precision era, Eur. Phys. J. C **75**, 132 (2015).
[80] R. D. Ball *et al.* (NNPDF Collaboration), Parton distributions for the LHC run II, J. High Energy Phys. 04 (2015) 040.
[81] T. Hahn, CUBA: A library for multidimensional numerical integration, Comput. Phys. Commun. **168**, 78 (2005).
[82] K. Fabricius, I. Schmitt, G. Kramer, and G. Schierholz, Higher order perturbative QCD calculation of jet cross-sections in $e + e-$ annihilation, Z. Phys. C **11**, 315 (1981).
[83] G. Kramer and B. Lampe, Jet cross-sections in $e + e-$ annihilation, Fortsch. Phys. **37**, 161 (1989).
[84] H. Baer, J. Ohnemus, and J. F. Owens, Next-to-leading-logarithm calculation of jet photoproduction, Phys. Rev. D **40**, 2844 (1989).
[85] B. W. Harris and J. F. Owens, The two cutoff phase space slicing method, Phys. Rev. D **65**, 094032 (2002).
[86] R. Ruiz, QCD corrections to pair production of type III seesaw leptons at hadron colliders, J. High Energy Phys. 12 (2015) 165.

[87] J. Alwall, R. Frederix, S. Frixione, V. Hirschi, F. Maltoni, O. Mattelaer, H.-S. Shao, T. Stelzer, P. Torrielli, and M. Zaro, The automated computation of tree-level and next-to-leading order differential cross sections, and their matching to parton shower simulations, J. High Energy Phys. 07 (2014) 079.

[88] G. F. Sterman, Summation of large corrections to short distance hadronic cross-sections, Nucl. Phys. **B281**, 310 (1987).

[89] S. Catani and L. Trentadue, Resummation of the QCD perturbative series for hard processes, Nucl. Phys. **B327**, 323 (1989).

[90] S. Catani and L. Trentadue, Comment on QCD exponentiation at large x, Nucl. Phys. **B353**, 183 (1991).

[91] S. Catani, M. L. Mangano, P. Nason, and L. Trentadue, The resummation of soft gluons in hadronic collisions, Nucl. Phys. **B478**, 273 (1996).

[92] M. Bonvini, S. Forte, and G. Ridolfi, Soft gluon resummation of Drell-Yan rapidity distributions: Theory and phenomenology, Nucl. Phys. **B847**, 93 (2011).

[93] S. Catani, D. de Florian, M. Grazzini, and P. Nason, Soft gluon resummation for Higgs boson production at hadron colliders, J. High Energy Phys. 07 (2003) 028.

[94] M. Bonvini, Resummation of soft and hard gluon radiation in perturbative QCD, arXiv:1212.0480.

[95] A. Alloul, N. D. Christensen, C. Degrande, C. Duhr, and B. Fuks, FeynRules 2.0—A complete toolbox for tree-level phenomenology, Comput. Phys. Commun. **185**, 2250 (2014).

[96] N. D. Christensen and C. Duhr, FeynRules—Feynman rules made easy, Comput. Phys. Commun. **180**, 1614 (2009).

[97] C. Degrande, C. Duhr, B. Fuks, D. Grellscheid, O. Mattelaer, and T. Reiter, UFO—The Universal FeynRules output, Comput. Phys. Commun. **183**, 1201 (2012).

[98] T. Sjöstrand, S. Ask, J. R. Christiansen, R. Corke, N. Desai, P. Ilten, S. Mrenna, S. Prestel, C. O. Rasmussen, and P. Z. Skands, An introduction to PYTHIA 8.2, Comput. Phys. Commun. **191**, 159 (2015).

[99] M. Cacciari and G. P. Salam, Dispelling the N^3 myth for the k_t jet-finder, Phys. Lett. B **641**, 57 (2006).

[100] M. Cacciari, G. P. Salam, and G. Soyez, FastJet user manual, Eur. Phys. J. C **72**, 1896 (2012).

[101] Y. L. Dokshitzer, G. D. Leder, S. Moretti, and B. R. Webber, Better jet clustering algorithms, J. High Energy Phys. 08 (1997) 001.

[102] M. Wobisch and T. Wengler, Hadronization corrections to jet cross-sections in deep inelastic scattering, arXiv:hep-ph/9907280.

[103] D. Alva, T. Han, and R. Ruiz, Heavy Majorana neutrinos from $W\gamma$ fusion at hadron colliders, J. High Energy Phys. 02 (2015) 072.

[104] G. Aad *et al.* (ATLAS Collaboration), Expected performance of the ATLAS experiment—Detector, trigger and physics, arXiv:0901.0512.

[105] V. Khachatryan *et al.* (CMS Collaboration), Search for heavy Majorana neutrinos in $e^{\pm}e^{\pm}+$ jets and $e^{\pm}\mu^{\pm}+$ jets events in proton-proton collisions at $\sqrt{8\ \mathrm{TeV}}$, J. High Energy Phys. 04 (2016) 169.

[106] Technical Report No. ATL-PHYS-PUB-2013-004, CERN (2013).

[107] K. Rehermann and B. Tweedie, Efficient identification of boosted semileptonic top quarks at the LHC, J. High Energy Phys. 03 (2011) 059.

[108] A. D. Martin, W. J. Stirling, R. S. Thorne, and G. Watt, Parton distributions for the LHC, Eur. Phys. J. C **63**, 189 (2009).

[109] J. C. Collins and D. E. Soper, Back-to-back jets in QCD, Nucl. Phys. **B193**, 381 (1981); **213**, 545(E) (1983).

[110] J. C. Collins and D. E. Soper, Back-to-back jets: Fourier transform from b to k_T, Nucl. Phys. **B197**, 446 (1982).

[111] J. C. Collins, D. E. Soper, and G. F. Sterman, Transverse momentum distribution in Drell-Yan pair and W and Z boson production, Nucl. Phys. **B250**, 199 (1985).

[112] H. n. Li, Unification of the k_T and threshold resummations, Phys. Lett. B **454**, 328 (1999).

[113] E. Laenen, G. F. Sterman, and W. Vogelsang, Higher Order QCD Corrections in Prompt Photon Production, Phys. Rev. Lett. **84**, 4296 (2000).

[114] E. Laenen, G. F. Sterman, and W. Vogelsang, Recoil and threshold corrections in short distance cross sections, Phys. Rev. D **63**, 114018 (2001).

[115] G. Bozzi, B. Fuks, and M. Klasen, Threshold resummation for slepton-pair production at hadron colliders, Nucl. Phys. **B777**, 157 (2007).

[116] S. Forte and G. Ridolfi, Renormalization group approach to soft gluon resummation, Nucl. Phys. **B650**, 229 (2003).

[117] G. Luisoni and S. Marzani, QCD resummation for hadronic final states, J. Phys. G **42**, 103101 (2015).

[118] M. Bonvini and S. Marzani, Resummed Higgs cross section at $\mathrm{N^3LL}$, J. High Energy Phys. 09 (2014) 007.

[119] M. Galassi *et al.*, GNU Scientific Library Reference Manual, 3rd ed. (Network Theory Limited, 2009).

[120] N. G. Deshpande, J. F. Gunion, B. Kayser, and F. I. Olness, Left-right symmetric electroweak models with triplet Higgs field, Phys. Rev. D **44**, 837 (1991).